Atmos. Chem. Phys. Discuss., 13, 4535–4600, 2013
www.atmos-chem-phys-discuss.net/13/4535/2013/
doi:10.5194/acpd-13-4535-2013

Atmospheric Chemistry and Physics Discussions

Global CO_2 fluxes estimated from GOSAT retrievals of total column CO_2

S. Basu[1,2], S. Guerlet[1], A. Butz[3], S. Houweling[1,2], O. Hasekamp[1], I. Aben[1], P. Krummel[4], P. Steele[4], R. Langenfelds[4], M. Torn[5], S. Biraud[5], B. Stephens[6], A. Andrews[7], and D. Worthy[8]

[1]SRON Netherlands Institute for Space Research, Utrecht, The Netherlands
[2]Institute for Marine & Atmospheric Research, Utrecht University, Utrecht, The Netherlands
[3]IMK-ASF, Karlsruhe Institute of Technology, Karlsruhe, Germany
[4]Commonwealth Scientific and Industrial Research Organisation, Victoria, Australia
[5]Lawrence Berkeley National Laboratory, California, USA
[6]National Center for Atmospheric Research, Colorado, USA
[7]National Oceanic and Atmospheric Administration, Colorado, USA
[8]Environment Canada, Toronto, Canada

Received: 30 November 2012 – Accepted: 5 February 2013 – Published: 18 February 2013

Correspondence to: S. Basu (s.basu@sron.nl)

Published by Copernicus Publications on behalf of the European Geosciences Union.

Abstract

We present one of the first estimates of the global distribution of CO_2 surface fluxes using total column CO_2 measurements retrieved from the Greenhouse gases Observing SATellite (GOSAT). We derive optimized fluxes from June 2009 to December 2010. We estimate fluxes from surface CO_2 measurements to use as baselines for comparing GOSAT data-derived fluxes. Assimilating only GOSAT data, we can reproduce the observed CO_2 time series at surface and TCCON sites in the tropics and the northern extra-tropics. In contrast, in the southern extra-tropics GOSAT X_{CO_2} leads to enhanced seasonal cycle amplitudes compared to independent measurements, and we identify it as the result of a land-sea bias in our GOSAT X_{CO_2} retrievals. A bias correction in the form of a global offset between GOSAT land and sea pixels in a joint inversion of satellite and surface measurements of CO_2 yields plausible global flux estimates which are more tightly constrained than in an inversion using surface CO_2 data alone. We show that assimilating the bias-corrected GOSAT data on top of surface CO_2 data (a) reduces the estimated global land sink of CO_2, and (b) shifts the terrestrial net uptake of carbon from the tropics to the extra-tropics. It is concluded that while GOSAT total column CO_2 provide useful constraints for source-sink inversions, small spatiotemporal biases – beyond what can be detected using current validation techniques – have serious consequences for optimized fluxes, even aggregated over continental scales.

1 Introduction

The traditional top-down approach for quantifying sources and sinks of CO_2 is an atmospheric inversion of CO_2 concentrations measured at the Earth's surface (Rödenbeck et al., 2003; Peters et al., 2007; Mueller et al., 2008; Chevallier et al., 2010; Gurney et al., 2008; Gurney, 2004). The measurements are performed by a network of trace gas monitoring stations established by various national agencies (Tans et al., 1990; Beardsmode and Pearman, 1987; Maki et al., 2011). For any given inversion

ACPD
13, 4535–4600, 2013

framework, the uncertainty bounds on regional CO_2 source-sink estimates depend heavily on the density of surface stations. The sparseness and spatial inhomogeneity of the existing surface network have limited our ability to understand the quantity and spatiotemporal distribution of CO_2 sources and sinks (Scholes et al., 2009). The difficulty of establishing surface stations in many areas that are interesting from a carbon cycle point of view – such as the Amazonian rain forest and the Arctic tundra – has prompted the development of space-based CO_2 sensors. Currently operational instruments such as the Infrared Atmospheric Sounding Interferometer (IASI, Crevoisier et al., 2009), the Operational Vertical Sounder (TOVS, Chédin et al., 2003), the Tropospheric Emissions Spectrometer (TES, Kulawik et al., 2010), and the Atmospheric Infrared Sounder (AIRS, Chahine et al., 2006), although sensitive to atmospheric CO_2, are not geared to studying surface sources and sinks of CO_2 due to their lack of sensitivity to near-surface CO_2. The Scanning Imaging Absorption Spectrometer for Atmospheric Cartography (SCIAMACHY) on board the ENVISAT satellite was the first space-based instrument to be sensitive to CO_2 in the lower troposphere (Reuter et al., 2011). More recent missions such as the Greenhouse Gas Observing Satellite (GOSAT, Hamazaki et al., 2004), and planned missions such as the Orbiting Carbon Observatory-2 (OCO2, Boesch et al., 2011) and the Active Sensing of CO_2 Emissions over Nights, Days, and Seasons (ASCENDS, Dobbs et al., 2007) have been and are being developed specifically to resolve surface sources and sinks of CO_2.

Several Observation System Simulation Experiments (OSSEs) have explored the added benefit of assimilating satellite measurements in atmospheric inversions of CO_2 (Rayner and O'Brien, 2001; Park and Prather, 2001; Houweling et al., 2004; Chevallier et al., 2007; Miller et al., 2007; Hungershoefer et al., 2010). These studies have shown that although space based measurements of CO_2 are not as accurate as surface layer measurements, the increased spatial coverage can provide information not available from the sparse surface network (Buchwitz et al., 2007). Whether this information can be harvested for source-sink inversions, however, depends on the specifics of the satellite instrument. Variations in CO_2 concentrations caused by surface fluxes

ACPD
13, 4535–4600, 2013

are damped by vertical transport, so satellite measurements that are sensitive to CO_2 at lower altitudes are better at constraining fluxes than measurements of CO_2 at higher altitudes. For example, Chevallier et al. showed that assimilating TOVS CO_2 observations in an inversion yielded unrealistic surface fluxes (Chevallier et al., 2005), and their attempt to assimilate AIRS radiances was outperformed by a standard surface data inversion (Chevallier et al., 2009). The poor performance of AIRS and TOVS in terms of constraining CO_2 surface fluxes can be traced to the fact that both these instruments are most sensitive to CO_2 in the upper troposphere ($\sim$ 150 hPa). More recently, Nassar et al. (2011) tried assimilating CO_2 measurements from the TES instrument which, with a spectral coverage of 3.2–15.4 µm, is sensitive to the mid-troposphere ($\sim$ 550 hPa). They showed that assimilating TES CO_2 in addition to surface CO_2 measurements improves constraints on surface fluxes, especially over regions absent from the surface network, such as the tropical forests of South America (Nassar et al., 2011). It follows that a satellite instrument sensitive to the lower troposphere would be even more useful for CO_2 source-sink inversions.

The Thermal And Near infrared Sensor for carbon Observation (TANSO) instrument on board the GOSAT satellite (Kuze et al., 2009) acquires CO_2 spectra in the 1.6 µm and 2.0 µm bands. It is therefore sensitive to the CO_2 concentration in the mid- to lower troposphere, and is thus sensitive to surface fluxes of CO_2. GOSAT has a polar orbit with a local overpass time of $\sim$ 13:00 and a three day repeat cycle. TANSO measures the intensity of reflected sunlight at the two CO_2 absorption bands mentioned before, and is therefore sensitive to the total column CO_2 between the surface and the top of the atmosphere within its footprint area of $\sim 80\,km^2$. We use the SRON-KIT RemoTeC retrieval algorithm to translate level 1 radiances to level 2 column averaged dry air CO_2 mole fractions, hereafter referred to as X_{CO_2} (Butz et al., 2011). RemoTeC is a "full physics" algorithm that simultaneously retrieves X_{CO_2}, X_{CH_4} and aerosol parameters needed to correct the optical path for the impact of scattering. The algorithm was evaluated by comparing the retrieved X_{CO_2} and X_{CH_4} with surface-based measurements of X_{CO_2} and X_{CH_4} from 12 stations of the Total Carbon Column Observing

ACPD
13, 4535–4600, 2013

Network (TCCON, Wunch et al., 2011). Compared to TCCON X_{CO_2}, RemoTeC X_{CO_2} has a single-shot precision of 2.5 ppm and a bias of −0.36 % averaged over all stations (Guerlet et al., 2013).

In this manuscript, we investigate the value of assimilating GOSAT X_{CO_2} in a source-sink inversion of CO_2 using RemoTeC retrievals of X_{CO_2}. We investigate whether there are obvious biases between RemoTeC X_{CO_2} and surface CO_2 measurements, and devise strategies to correct for those biases to jointly assimilate X_{CO_2} and surface CO_2 data. We check if the addition of X_{CO_2} constraints on top of surface CO_2 data reduces the uncertainty on estimated fluxes from an atmosheric inversion, especially over areas with scant surface data. Most importantly, we look for portions of the carbon cycle about which our knowledge changes quantitatively when we jointly assimilate X_{CO_2} and surface CO_2, compared to a surface-only inversion.

This idea of jointly assimilating observations from satellites and surface networks has been found to be more beneficial than assimilating either type of observation individually (Hungershoefer et al., 2010; Chevallier et al., 2009). Surface measurements of CO_2 are in general more accurate than satellite measurements, so a given number of surface observations provide a tighter constraint on surface fluxes than the same number of satellite observations. Satellite measurements, on the other hand, have a wider coverage, and therefore provide constraints on CO_2 in areas devoid of surface stations. Even in areas with a high density of surface stations, surface CO_2 and X_{CO_2} measurements can impose different constraints on surface fluxes, resulting in, for example, different amplitudes for the estimated seasonal cycle in the net ecosystem exchange (Yang et al., 2007; Basu et al., 2011; Keppel-Aleks et al., 2012).

A joint assimilation of surface CO_2 and satellite X_{CO_2} measurements can potentially compensate for spatiotemporal biases in the satellite instrument using ground data from background stations. Since most space-based CO_2 sensors are one of a kind, each comes with its own bias characteristics, which can vary seasonally, and with latitude, and can drift during the lifetime of the instrument. These biases can be partly compensated by assimilating background surface stations – such as Mauna Loa and

ACPD
13, 4535–4600, 2013

South Pole – which provide accurate information on large-scale spatial gradients and long term temporal trends of CO_2.

The GOSAT X_{CO_2} data record starts from April 2009. In this work, we assimilate both surface and GOSAT data between 1 June 2009 and 1 January 2011, to optimize the surface flux of CO_2 between 1 June 2009 and 1 December 2010. The structure of this manuscript is as follows. In Sect. 2, we describe the satellite and surface data assimilated in our inversions. In Sect. 2.1 we describe the selection procedure for surface measurements and the temporal averaging employed. In Sect. 2.2 we describe the X_{CO_2} retrievals used, and in particular how errors are ascribed to individual soundings, which is crucial for striking the right balance between satellite and surface data. In Sect. 3 we describe the TM5 4DVAR atmospheric inversion system, with particular focus on the prior fluxes used in Sect. 3.1.1, the initial atmospheric CO_2 field in Sect. 3.1.3, and the estimation of the posterior covariance matrix in Sect. 3.2. Section 3.3 describes how we validate our optimized fluxes by comparing the resultant atmospheric CO_2 signal with aircraft measurements from the CONTRAIL campaign and X_{CO_2} measurements from the TCCON network. Sensitivity runs to test the robustness of our optimization approach are described in Sect. 3.4. Section 4 contains the results of our atmospheric inversions, with Sect. 4.2 devoted to validation. Section 4.3 is where we present the estimated fluxes themselves, including large-scale aggregates and seasonal time series. In Sect. 4.4 we present the results of the sensitivity tests proposed in Sect. 3.4. Finally, we discuss the implications of our findings in Sect. 5.

2 Assimilated data

We assimilate both boundary layer CO_2 measurements, i.e. from surface flasks and in situ measurements, and GOSAT X_{CO_2}. In order to derive optimized fluxes from 1 June 2009 to 1 December 2010, we added three months of spin-up and one month of spin-down time, resulting in a model run from 1 March 2009 to 1 January 2011. However, we did not put any observational constraints during the spin-up time, and thus our

ACPD
13, 4535–4600, 2013

assimilated data – both surface and satellite – span the period from 1 June 2009 to 1 January 2011. The two data streams are described in detail below.

2.1 Point samples

We assimilate 16 887 CO_2 surface layer observations – referred to as "point samples" since each one represents the CO_2 concentration at a point in space and time – chosen from the set of observations assimilated in CarbonTracker 2011 (http://carbontracker.noaa.gov, observations retrieved from ftp://aftp.cmdl.noaa.gov/products/carbontracker/co2/CT2011/observations/). The observations come from 132 distinct locations, which are shown in Fig. 1. The samples include data from nine tall towers (all within the continental US), thirteen in situ monitoring stations (seven from Environment Canada, two from the National Center for Atmospheric Research, and four from the National Oceanic and Atmospheric Administration), and sixty three surface flask sites operated by various agencies. For tall towers having multiple intake levels, only the concentrations sampled from the highest levels are assimilated (Peters et al., 2007), such as the 396 m (above ground) level of the WLEF tower near Park Falls, Wisconsin.

Hourly CO_2 records were available from several CO_2 monitoring sites. However, assimilating the full hourly CO_2 record leads to model biases, especially at night (Patra et al., 2008). Following the prescription of Peters et al. (2010), we create at most one observation per station per day, representative of the largest possible footprint for that station. For low altitude stations, observations with the largest footprints are those collected when the daytime planetary boundary layer (PBL) is well developed and at its highest, which is during the mid to late afternoon. For mountaintop sites on the other hand, the largest footprint corresponds to the time when the observations sample free tropospheric air and the nighttime PBL is at its lowest, i.e. after midnight. Hence, depending on the station location, we assimilate either late afternoon or late night CO_2 data. Data collected are averaged within a four hour time window to get rid of high frequency fluctuations that our coarse transport model cannot possibly resolve. During

ACPD
13, 4535–4600, 2013

the data assimilation phase, the modeled CO_2 concentration at a site is also averaged over the same four hour period before being compared to observations from that site.

2.2 Satellite measurements

X_{CO_2} data used in this work were retrieved from GOSAT soundings using the RemoTeC algorithm. RemoTeC is being jointly developed at the Netherlands Institute for Space Research (SRON) and the Karlsruhe Institute of Technology (KIT). Its performance has been extensively evaluated through retrieval simulations, in particular with respect to its capability to account for lightpath modification by particle scattering in the atmosphere (Butz et al., 2010, 2009, 2012). Initial validation against ground-based observations by TCCON has shown very promising data quality with respect to precision and accuracy of data.

Out of the 262 355 X_{CO_2} soundings retrieved by RemoTeC within our observation window, we assimilated 77 769 that passed RemoTeC quality checks. The assimilated X_{CO_2} observations, shown in Fig. 2 to give an idea of the coverage, include both land and ocean soundings, where the latter were acquired in GOSAT's ocean glint observation mode. RemoTeC quality checks rely on a series of criteria described in Butz et al. (2011). GOSAT observations are screened for instrument malfunction, suitable observation geometry, signal-to-noise, (cirrus) cloud contamination, and surface elevation variability of the observed scene before they are submitted to the retrieval. Data recorded in the "medium gain" mode of TANSO-FTS – typically collected over bright surfaces such as deserts – are discarded since a scan speed instability of the FTS affects data quality. Together with X_{CO_2} (and X_{CH_4}), RemoTeC delivers a range of retrieval diagnostics that allow for a posteriori quality assessment, among them standard criteria such as the posterior χ^2 and degrees of freedom for signal. The retrieved particle scattering properties of the atmosphere hint on the difficulty of the observed scene in terms of lightpath modification through aerosol and cirrus particles. The retrieval diagnostics, along with the retrieved particle scattering properties, were used to select the 77 769 scenes mentioned above which were assimilated. Before data assimilation,

ACPD
13, 4535–4600, 2013

a bias correction based on coincident TCCON soundings was applied to the 77 769 X_{CO_2} measurements, as detailed by Guerlet et al. (2013).

Going by the number of samples, it would seem that satellite data provide ∼4.5 times as much information to our inversion compared to surface data. That is, however not the case since not all 77 769 soundings are independent. Errors in different X_{CO_2} retrievals could be correlated, for example, due to errors in ancillary data – such as meteorological fields and spectral line shapes – used in retrievals (see, e.g. Fig. 2 of Chevallier et al., 2005). Since observed X_{CO_2} values are assimilated by comparing them with simulated X_{CO_2} from an atmospheric transport model, the transport model can also generate correlations between observations (Kaminski et al., 2001). While accounting properly for these correlations in a Bayesian inversion is crucial, in reality the correlations are hard to estimate, and difficult to implement in an inversion framework. In lieu of a full observation error covariance matrix, which is formally $n_{obs} \times n_{obs}$ where $n_{obs} \sim 10^5$ is the number of observations assimilated, data assimilation systems typically use any of a variety of techniques such as binning, data thinning and error inflation to construct a diagonal approximation of the full matrix, which is easier to implement. Of these approximations, error inflation was shown to perform best in the context of assimilating satellite X_{CO_2} for estimating CO_2 sources and sinks (Chevallier, 2007). They showed that multiplying all observation errors by 2 yielded optimized surface fluxes closest to the exact solution using the full error covariance matrix.

In our inversion system, we also inflate X_{CO_2} errors to account for correlated observation errors. However, unlike Chevallier (2007), we do not inflate all errors by the same factor. For an observation i with reported retrieval error σ_i, we consider all N observations within distance R and time T of i. If all these observations were perfectly correlated, and we averaged them, then the average observation would have an error σ_b

ACPD
13, 4535–4600, 2013

$$\sigma_b^2 = \frac{1}{N}\left[\sum_{j=1}^{N}\sigma_j\right]^2$$

On the other hand, if all N observations were uncorrelated and we inflated their errors by α_i and then averaged them, that average would have an error σ_{uncorr}

$$\sigma_{\text{uncorr}}^2 = \frac{1}{N}\sum_{j=1}^{N}\alpha_i^2\sigma_j^2$$

If we demand $\sigma_b = \sigma_{\text{uncorr}}$, then we get the inflation factor α_i for the error σ_i

$$\alpha_i^2 = \frac{\left(\sum_{j=1}^{N}\sigma_j\right)^2}{\sum_{j=1}^{N}\sigma_j^2} \quad (1)$$

This approach has the benefit that errors of observations that are clustered together are inflated more than of those that are far away from each other, effectively de-weighting clustered observations. This is physically plausible, since errors in observations closer together are expected to be more strongly correlated, resulting in fewer effective constraints. Applied to our X_{CO_2} dataset, this algorithm results in inflation factors between 1 and 6.

3 The Inversion System

We assimilate surface CO_2 and GOSAT X_{CO_2} observations in a 4DVAR system to estimate monthly surface fluxes. The inversion system closely follows the framework described in Meirink et al. (2008). We describe it briefly below, and the reader is encouraged to refer to Meirink et al. (2008) for details of the TM5 4DVAR system.

ACPD
13, 4535–4600, 2013

3.1 TM5 4DVAR

Let $\boldsymbol{x}$ denote a vector of length N representing surface fluxes, $\boldsymbol{y}$ a vector of length M of atmospheric observations available to constrain the fluxes, and let $\boldsymbol{x}_0$ be a prior estimate of surface fluxes before any observations are made. We estimate the optimal value of $\boldsymbol{x}$, given a prior guess $\boldsymbol{x}_0$ and observations $\boldsymbol{y}$, by minimizing the cost function

$$J = \frac{1}{2}(H\boldsymbol{x} - \boldsymbol{y})^T R^{-1}(H\boldsymbol{x} - \boldsymbol{y}) + \frac{1}{2}(\boldsymbol{x} - \boldsymbol{x}_0)^T B^{-1}(\boldsymbol{x} - \boldsymbol{x}_0) \quad (2)$$

where H is the composition of an atmospheric transport operator and an observation operator, R is the observation error covariance matrix and B is the prior flux covariance matrix,

$$R = \left\langle (\boldsymbol{y} - \bar{\boldsymbol{y}})(\boldsymbol{y} - \bar{\boldsymbol{y}})^T \right\rangle$$

$$B = \left\langle (\boldsymbol{x}_0 - \bar{\boldsymbol{x}}_0)(\boldsymbol{x}_0 - \bar{\boldsymbol{x}}_0)^T \right\rangle$$

where $\bar{\boldsymbol{a}}$ denotes the ensemble average of $\boldsymbol{a}$, i.e. the average over a number of realizations of $\boldsymbol{a}$. We divide the CO_2 flux into four categories, similar to Peters et al. (2007). The flux from surface grid cell i_{hor} at time t is

$$\boldsymbol{x}(i_{\text{hor}}, t) = \boldsymbol{x}^{\text{bio}}(i_{\text{hor}}, t) + \boldsymbol{x}^{\text{oce}}(i_{\text{hor}}, t) + \boldsymbol{x}^{\text{FF}}(i_{\text{hor}}, t) + \boldsymbol{x}^{\text{fire}}(i_{\text{hor}}, t) \quad (3)$$

where the superscripts denote: "bio" = flux from terrestrial biosphere, "oce" = flux from oceans, "FF" = fossil fuel emissions, and "fire" = flux from biomass burning and land use change. The flux from each category is specified on a global $6^\circ \times 4^\circ$ grid every three hours. $\boldsymbol{x}^{\text{FF}}$ and $\boldsymbol{x}^{\text{fire}}$ are not optimized; $\boldsymbol{x}^{\text{bio}}$ and $\boldsymbol{x}^{\text{oce}}$ are optimized on a global $6^\circ \times 4^\circ$ grid every month for 22 months. Thus, the size of the state vector is $N = 2 \times 60 \times 45 \times 22 = 118\,800$.

ACPD
13, 4535–4600, 2013

3.1.1 Prior flux x_0 and flux covariance B

A priori estimates of $\boldsymbol{x}^{\text{bio}}$ and $\boldsymbol{x}^{\text{fire}}$ are taken from CASA GFED3 (van der Werf et al., 2010). $\boldsymbol{x}^{\text{fire}}$ denotes the CO_2 emitted directly due to the burning of vegetation in forest fires, whereas the after effects of the fire – e.g. rotting litter, decaying dead trees – are bundled into the biosphere estimate $\boldsymbol{x}^{\text{bio}}$ through heterotrophic respiration (R_H). In the present state of our knowledge, the uncertainty in $\boldsymbol{x}_0^{\text{fire}}$ is much smaller than the uncertainty in $\boldsymbol{x}_0^{\text{bio}}$, and hence we choose to hold $\boldsymbol{x}^{\text{fire}}$ fixed at its prior, inventory-based value, while absorbing small variations in $\boldsymbol{x}^{\text{fire}}$ into the much more uncertain $\boldsymbol{x}^{\text{bio}}$. CASA GFED3 provides monthly net primary production (NPP) and R_H, from which the net ecosystem exchange NEE = R_H – NPP is calculated. Higher frequency variations – such as the diurnal cycle – are added to NEE every three hours using a relation involving Q_{10} and incident solar radiation as described in Olsen and Randerson (2004).

A priori estimates of $\boldsymbol{x}^{\text{oce}}$ come from an ocean interior inversion described in Jacobson et al. (2007). This inversion yields monthly mean oceanic CO_2 fluxes, which are combined with 3-hourly surface pressures and 10 m winds from the ECMWF ERA 40 model to give synoptic variations and interannual variability as described in Kettle and Merchant (2005).

Fossil fuel emissions $\boldsymbol{x}^{\text{FF}}$, which are held fixed at their prior values in our inversion, come from a combination of several inventories. The procedure for compiling $\boldsymbol{x}_0^{\text{FF}}$ is identical to the fossil fuel module described in the CarbonTracker documentation (CarbonTracker, 2012), except that we do not use the ODIAC database. Annual global total fossil fuel emissions up to 2008 are taken from Boden et al. (2010) and are extrapolated to 2009 and 2010 using BP Statistical Review of World Energy as described by Myhre et al. (2009). The total emission from a country is distributed within the country according to the spatial pattern of the higher resolution EDGAR v4.0 inventory from the European Commission. Where available, a seasonal cycle is imposed on the annual total data, for example by using the monthly data from Blasing et al. (2005).

ACPD
13, 4535–4600, 2013

For the two flux categories being optimized, $\boldsymbol{x}^{\text{bio}}$ and $\boldsymbol{x}^{\text{oce}}$, we need to specify a spatiotemporal covariance matrix for the prior flux, i.e. the matrix B in Eq. (2). We assume that the covariance is separable in space and time, so that

$$\text{cov}(x_{\boldsymbol{r}_1,t_1}, x_{\boldsymbol{r}_2,t_2}) = \sigma_{\boldsymbol{r}_1,t_1}\sigma_{\boldsymbol{r}_2,t_2} C_{\boldsymbol{r}}(\boldsymbol{r}_1,\boldsymbol{r}_2) C_t(t_1,t_2) \quad (4)$$

where $x_{\boldsymbol{r},t}$ is the CO_2 flux from position $\boldsymbol{r}$ at time t. We choose correlation functions $C_{\boldsymbol{r}}$ and C_t to be exponentially decaying with characteristic length and time scales L and T respectively:

$$C_{\boldsymbol{r}}(\boldsymbol{r}_1,\boldsymbol{r}_2) = e^{-|r_1-r_2|/L} \qquad C_t(t_1,t_2) = e^{-|t_1-t_2|/T}$$

Further, we assume no prior correlation between the two optimized categories, biosphere and oceanic fluxes, so each category is characterized by its own L and T. The standard deviation $\sigma_{\boldsymbol{r},t}$ is specified as a certain fraction ξ of the absolute flux from $(\boldsymbol{r},t)$,

$$\sigma_{\boldsymbol{r},t} = \max\left(\xi \left| x_{\boldsymbol{r},t} \right|, \sigma_0\right)$$

where $\sigma_0 = 0.005\,\text{kg}\,CO_2\,\text{sec}^{-1}\,\text{gridbox}^{-1}$ allows the inversion to adjust fluxes over gridboxes with zero prior emission. Each category has its own ξ, and the category-specific parameters are summarized in Table 1.

For each category, the parameters in Table 1 were tuned to produce the same ratio of annual flux uncertainty to annual mean flux as seen in the prior fluxes of CarbonTracker 2011, which were 1.20 and 0.51 for the terrestrial and oceanic components respectively.

3.1.2 Transport and observation operator *H*

CO_2 surface fluxes were propagated forward in time using the TM5 atmospheric transport model run on a global $6^\circ \times 4^\circ$ grid over 25 vertical layers (Krol et al., 2005). We drove TM5 with ECMWF ERA Interim meteorological data, which were coarsened from

ACPD
13, 4535–4600, 2013

their original resolution to our model grid. Since the CO_2 mixing ratio in a 3-dimensional grid cell is only representative of the average mixing ratio inside that cell, the mixing ratio at each point sample location was calculated by linear interpolation using the tracer mass and its spatial gradient, both of which are calculated by TM5. A similar linear interpolation in two dimensions was performed when calculating the modeled total column at a satellite sounding location.

For comparing to X_{CO_2} measurements, the modeled CO_2 column needs to be convolved with the satellite averaging kernel. For this, the column of modeled CO_2 mixing ratio c^{mod} at the time and position of a satellite sounding was first re-binned onto the retrieval grid by multiplying with a redistribution matrix h, then convolved with the averaging kernel A and added to the prior profile c^{pri} to yield the modeled total column

$$X_{CO_2}{}^{\mathrm{mod}} = w^T A\,(hc^{\mathrm{mod}} - c^{\mathrm{pri}}) + w^T c^{\mathrm{pri}} \quad (5)$$

where w is a vector of pressure weights, w_i = mass of dry air in layer i/mass of dry air in total column, and c^{pri} is the prior CO_2 profile used in the retrieval.

3.1.3 Initial atmospheric CO_2 field

The transport model TM5 simulates atmospheric CO_2 concentrations given a flux scenario and a 3-dimensional CO_2 field at the model starting time, the so-called initial concentration, which is not optimized in our inversions. While small biases due to an incorrect initial concentration can be compensated by surface fluxes during the spin-up period (for us, 1 March–1 June 2009), large biases cannot be corrected in three months and will result in erroneous fluxes over the first few months of our assimilation window. Therefore, it is important to start with an initial concentration field consistent with the state of the atmosphere as captured by our assimilated measurements.

We perform an optimization with only surface CO_2 measurements as described in Sect. 2.1 from 1 January 2008 to 1 May 2009, following the same methodology detailed in this section. The initial concentration for that 4DVAR run is taken from the posterior

ACPD
13, 4535–4600, 2013

dry air CO_2 mole fraction field of CarbonTracker 2010 on 1 January 2008. The optimized posterior flux over the 16 months is then propagated forward in TM5 to create an optimized atmospheric CO_2 field. This CO_2 field is sampled at 00:00 UTC on 1 March 2009 to create the initial concentration field that is used in our inversions described in the rest of this manuscript. By stopping the 16 month assimilation on 1 May 2009, we make sure that no observation is counted twice, since the inversions presented later assimilate observations made after 1 June 2009.

3.1.4 Observations *y* and observation error covariance *R*

Observations used in Eq. (2) come from one or both of the streams described in Sect. 2. After error inflation (for satellite data) and temporal averaging (for point samples), the observations are assumed to be independent, so R is diagonal, with elements

$$R_{ii} = \sigma^2_{\text{obs},i} + \sigma^2_{\text{mod},i}$$

where $\sigma_{\text{obs},i}$ is the estimated error in observation i (after error inflation, in the case of X_{CO_2}), and $\sigma_{\text{mod},i}$ is the estimated error in modeling the i-th observation. The latter component, which is the so-called model representativeness error, is the error made by our finite resolution model in simulating a sample at a specific location. This error will be large in an area with a large spatial gradient of CO_2, and will be small if the CO_2 concentration in an area is spatially uniform. For point observations, we estimate this error for a grid cell as the standard deviation in CO_2 mixing ratio across all neighbouring grid cells in three dimensions. In case of boundary cells such as surface cells or cells at the poles, the concentration in the non-existent neighbor is simulated by

$$c_{\text{neighbor}} = c_{\text{cell}} + \boldsymbol{d} \cdot \nabla c$$

where $\boldsymbol{d}$ is the vector from cell's center to the center of its (missing) neighbor. In the case of point samples, due to the high accuracy of flask and in situ measurements, $\sigma_{\text{mod},i} > \sigma_{\text{obs},i}$ for most observations.

ACPD
13, 4535–4600, 2013

In the case of satellite measurements, the model representativeness error is calculated for each gridbox (as above) in the modeled column c^{mod}. Let the error in the i-th vertical gridbox in column c^{mod} be e_i. Then σ_{mod} for the modeled X_{CO_2} is calculated by

$$\sigma^2_{\text{mod}} = \sum_i \left(w^T A\, h\right)^2_i e^2_i$$

For the TM5 transport model running at $6^\circ \times 4^\circ$ lateral resolution and 25 vertical layers, for point samples, the mean σ_{mod} is 3 ppm, larger than the mean σ_{obs} of 2.5 ppm. For satellite observations, the mean σ_{mod} of 0.05 ppm is smaller than the mean σ_{obs} of 3.6 ppm. It should be noted that $\bar{\sigma}_{\text{obs}} = 2.5$ ppm for point samples is not much smaller than the $\bar{\sigma}_{\text{obs}} = 3.6$ ppm for satellite samples, contrary to the expectation that point samples are much more accurate than satellite samples. This is because the σ_{obs} for satellite samples reflects the estimated error for individual soundings, whereas σ_{obs} for point samples includes the CO_2 variability over a four hour window that each point sample is supposed to represent. A single point sample is of course much more accurate, with an estimated error of ~ 0.2 ppm.

3.2 The minimization algorithm and the posterior covariance matrix

To minimize the cost function J in Eq. (2), we use the adjoint TM5 transport model and adjoint point and satellite observation operators to calculate $\nabla_x J$ (Tarantola, 2005). Details of constructing the adjoint model are given in (Meirink et al., 2008) and references therein. Since our problem is linear, i.e. J is a purely quadratic function of $\boldsymbol{x}$, we use the conjugate gradient algorithm for minimizing J (Navon and Legler, 1987). The application of the algorithm specifically to a 4DVAR data assimilation problem is described by Fisher and Courtier (1995). The method is based on the Lanczos algorithm (Lanczos, 1950) for solving a linear system and allows us to simultaneously minimize J and derive the leading eigenvalues and eigenvectors of the Hessian $\nabla^2_x J$. Section 2.2 of Meirink et al. (2008) describes how the algorithm is used in a flux inversion system to

ACPD
13, 4535–4600, 2013

estimate optimized fluxes as well as the posterior covariance matrix. We summarize it very briefly below.

The optimization is performed in terms of a preconditioned variable z (Courtier et al., 1994)

$$z = Lz + x_0 \qquad B = LL^T$$

The Hessian in this preconditioned space is

$$\mathcal{H} = \frac{\partial^2 J}{\partial z^2} = I + L^T H^T R^{-1} H L$$

The optimization, after n steps, yields the n leading eigenvalues $\lambda_{i=1\ldots n}$ and the corresponding eigenvectors $\boldsymbol{v}_{i=1\ldots n}$ of $\mathcal{H}$. These can be used to derive an approximation to the posterior covariance matrix $\hat{B}$

$$\hat{B} = B + \sum_{i=1}^{n} \left(\frac{1}{\lambda_i} - 1 \right) (L\boldsymbol{v}_i)(L\boldsymbol{v}_i)^T \tag{6}$$

At the start of the optimization, $n = 0$ and posterior error estimates are as large as prior estimates, or $\hat{B} = B$. During an optimization, the λ's start from a high positive value and approach 1 as $n \rightarrow N$. Hence with each iteration the posterior covariance matrix is reduced by some amount, but the reduction becomes less and less as $\lambda \rightarrow 1$, until $\hat{B}$ reaches its exact value at $n = N$. In all the inversions reported in this paper, the lowest eigenvalue $1 < \lambda_{\min} < 1.03$, and hence our reported flux uncertainties are close to but slightly higher than those estimated from the exact posterior covariance matrix. Uncertainty estimates of spatiotemporally aggregated fluxes, e.g. the global total annual CO_2 emission, can be calculated by summing up the correct elements of $\hat{B}$.

Due to the high dimensionality of the problem, exact convergence is never reached, and we stop the conjugate gradient iterations when

$$|\nabla_x J| \leq \eta |\nabla_x J(x_0)|$$

ACPD
13, 4535–4600, 2013

where $\eta = 10^{-8}$ is a small scalar constant.

3.3 Validation of the optimized fluxes

Our flux inversion is an underconstrained problem, i.e. there are fewer measurements than degrees of freedom that need constraining. Therefore, given a prior flux and a set of observations, the optimization will always converge to some optimized posterior flux, which could be quite far from the true flux scenario. A flux inversion should ultimately be judged on how well it can reproduce the atmospheric state of the relevant tracer, which, in our case, is captured by measurements of atmospheric CO_2 concentration. We evaluate our inversions by simulating the atmospheric CO_2 field with posterior flux estimates, and comparing that field with independent CO_2 measurements, i.e. measurements that have not been assimilated by the 4DVAR system. We use two types of measurements, point and total column.

3.3.1 Point samples from CONTRAIL

The Comprehensive Observation Network for TRace gases by AIrLiner (CONTRAIL) project (Machida et al., 2008) has been observing vertical CO_2 profiles over 43 airports worldwide and along intercontinental flight paths using five Japan Airlines (JAL) commercial airliners. The data coverage is extensive in the Northern Hemisphere, and vertically the samples go up to 150 hPa (Sawa et al., 2012; Niwa et al., 2012). We sample our posterior atmospheric CO_2 field at 967 418 points between 1 June 2009 and 1 January 2011 corresponding to CONTRAIL samples available. The sampling algorithm and model error calculation is identical to our point sampling step during assimilation, detailed in Sect. 3.1.4.

ACPD
13, 4535–4600, 2013

3.3.2 X_{CO_2} samples from TCCON

The Total Carbon Column Observation Network (TCCON) measures X_{CO_2} at 22 sites globally (Wunch et al., 2011, 2010), a number of which were operational during the time window of our inversion. We sample the posterior atmospheric CO_2 field at 235 467 sampling times and locations between 1 June 2009 and 1 January 2011 corresponding to TCCON samples available. In each case, we convolve our vertical CO_2 profile with the relevant TCCON averaging kernel and add the appropriate TCCON prior CO_2 profile. At most times, the time series of individual X_{CO_2} soundings has a lot of variability that can obscure the picture if we are interested in phenomena such as the summer drawdown of CO_2, which happens over several weeks. Therefore, for each site, all the observations and modeled samples have been averaged over seven days to get rid of high frequency variations.

3.4 Robustness of the optimized fluxes

There are many sources of error in the 4DVAR inversion system, of which only two – namely, error in the specification of prior fluxes (B in Eq. 2), and error in simulating observations (R in Eq. 2) – are explicitly incorporated in the data assimilation system. Our final flux estimates and the associated error bounds reflect the uncertainties introduced by these two error sources. There are other, more systematic errors, however, that are not accounted for by $\hat{B}$ in Eq. (6). The most critical of them are systematic errors in atmospheric tracer transport, of which there could be many sources, such as finite spatiotemporal resolution, incorrect vertical transport, systematic errors in the driving meteorological fields, and incorrect interhemispheric exchange rates. In this work, we have investigated the impact of some of these errors by running the following sensitivity tests, the results of which we present in Sect. 4.4:

1. We changed the vertical resolution from 25 layers to 60 layers, the maximum vertical resolution available for ECMWF Era Interim meteorological data. Changing

ACPD
13, 4535–4600, 2013

the vertical resolution changes the vertical transport. This test therefore quantifies the sensitivity of estimated fluxes to errors in vertical transport.

2. We changed the horizontal resolution from $6^\circ \times 4^\circ$ to $3^\circ \times 2^\circ$ globally. This test addresses the sensitivity of optimized fluxes to the finite spatiotemporal resolution of our transport model.

3. We changed the driving meteorological data from ECMWF Era Interim to ECMWF operational forecasts. This is equivalent to using a different transport model (Wang et al., 2009), and thus explores the sensitivity of our estimated fluxes to our choice of simulated atmospheric transport.

All three changes above also modify the interhemispheric exchange rate. So the above tests also test the robustness of inversion-derived flux estimates to changes in interhemispheric transport.

4 Inversion results

4.1 Consistency between surface and GOSAT CO_2

We first check whether there are obvious biases between GOSAT X_{CO_2} and surface samples by looking at the atmospheric state of CO_2 estimated after assimilating only GOSAT soundings. We compare the posterior CO_2 time series at surface stations in the northern extra-tropics and tropics to observations at those stations in Fig. 3. An inversion using only GOSAT X_{CO_2} can reproduce the surface time series of CO_2 faithfully, the average model-observation bias decreasing from a prior value of 1.95 ppm to −0.55 ppm. In the northern extra-tropics, the prior time series do not have sufficiently deep minima in the summer due to too little uptake in the CASA fluxes (Yang et al., 2007). The top row of Fig. 3 shows that assimilating GOSAT X_{CO_2} corrects for that underestimated uptake. The phasing of the seasonal cycle is also spot-on, even at difficult sites with a very active biosphere such as Park Falls. In the tropics (lower row in Fig. 3),

ACPD
13, 4535–4600, 2013

the seasonal cycle is not as prominent, but we still see a GOSAT-only inversion being closer to the observed time series than prior estimates. Although we have shown four stations for brevity, the good agreement between a GOSAT-only inversion and surface stations is prevalent throughout stations in the tropics and the northern extra-tropics. This positive outcome was by no means obvious at the start of the GOSAT mission, and bodes well for the future of constraining the carbon cycle by remote sensing.

In the southern extra-tropics, however, the picture is not as nice. As shown in Fig. 4, assimilating only GOSAT data overestimates the seasonal cycle. We will see later in Sect. 5 that this stems at least partly from X_{CO_2} retrieval problems over the ocean, which we are still working on improving.

4.2 Validation of CO_2 concentration derived from optimized fluxes

4.2.1 Comparison to CONTRAIL

Figure 5 shows monthly averages of CONTRAIL observations in the northern temperate latitudes and the tropics, defined respectively as 23.5° N–66.5° N and 23.5° S–23.5° N, along with posterior CO_2 concentrations from several inversions sampled at CONTRAIL locations and times. As can be seen in Fig. 5, all inversions produce improved states of the atmosphere compared to the prior.

In the northern temperate latitudes, GOSAT data point to a deeper drawdown of CO_2 compared to surface data in the summer of 2009, and a higher outgassing in DJF 2009–2010. We will see in Sect. 4.3 that, as expected, assimilating GOSAT X_{CO_2} leads to an amplified seasonal cycle in the surface flux. Since the CONTRAIL data do not show a similar amplification – in fact, the CONTRAIL data follow the surface-only inversion quite closely – this enhanced seasonal cycle need not be a real feature of the surface flux. Whether this enhancement is something specific to the 2009–2010 seasonal cycle or is a more general result of assimilating GOSAT data can only be resolved from multi-year GOSAT assimilations in the future.

ACPD
13, 4535–4600, 2013

In the tropics, assimilating GOSAT data results in a CO_2 drawdown in the NH summer of 2009 that is not reflected in the CONTRAIL data. On the other hand, CONTRAIL CO_2 points to an outgassing in the NH spring of 2010 that is better captured by GOSAT than by surface samples. This is also seen in the tropical surface flux time series in Sect. 4.3. It is tempting to investigate whether the enhanced seasonal cycle in the southern extra-tropics as seen in Fig. 4 is observed in comparisons to CONTRAIL data as well, but unfortunately the lack of CONTRAIL samples at those latitudes makes such a comparison impossible.

4.2.2 Comparison to TCCON

To evaluate the inversions against TCCON, both TCCON data and co-sampled optimized X_{CO_2} were averaged over 7 day windows to improve visual clarity. The resulting time series are plotted in Fig. 6 (left and center) for the northern and Southern Hemisphere stations reporting the maximum number of data points over our assimilation time window. Due to data gaps in different TCCON stations over Europe, data from four TCCON stations were combined in Fig. 6 (right). For each station, coincident GOSAT data were chosen based on a sampling procedure by Oshchepkov et al. (2012). First, all GOSAT soundings within ±15° longitude and ±7.5° latitude of a station were selected. Of those, soundings were deemed coincident with the TCCON station if the modeled X_{CO_2} at the sounding locations were within 0.5 ppm of the modeled X_{CO_2} over the TCCON station. Details of the co-location technique have been discussed by Guerlet et al. (2013). The coincident GOSAT data were averaged over 15 days (owing to higher scatter) and plotted with a star symbol. The shaded region around a GOSAT data point denotes the spread of coincident GOSAT data during an averaging period.

At Lamont, the TCCON data in the summer of 2009 show a drawdown of CO_2 which is mirrored in the GOSAT data and in inversions with GOSAT data, but not in inversions with surface data (Fig. 6, left). This points to enhancements of the summer uptake over the continental United States or upwind areas that are not captured by surface CO_2 data. In the future, with the availability of multi-year GOSAT datasets, we will investigate

ACPD
13, 4535–4600, 2013

whether 2009 had anomalously high uptake or whether the mismatch between surface and GOSAT inversions persists year after year.

A similar enhancement is not seen at European TCCON stations; an inversion of only surface data reproduces the summer 2009 drawdown seen by TCCON stations quite well (Fig. 6, right). Thus the enhanced depletion of summer 2009 CO_2 higher up, which is sensed by GOSAT over North American TCCON stations, is a regional/continental scale phenomenon rather than one occuring across the entire latitude band. This is consistent with the fact that CONTRAIL samples over the northern temperate latitudes (Fig. 5, left) do not see an enhanced depletion of CO_2 when compared with a surface-only inversion.

At Wollongong, the bias between TCCON and co-located GOSAT data is seen to vary seasonally. Apart from a small overall high bias in coincident GOSAT X_{CO_2}, the GOSAT data in July–August 2010 is higher than TCCON by $\sim$2 ppm, whereas in March–April 2009 it is higher by $\sim$1 ppm. This seasonal variation in the bias enhances the seasonal cycle of the inverted fluxes in the southern temperate latitudes, which is consistent with the enhanced seasonal cycle of CO_2 seen at surface stations in Fig. 4.

4.3 Optimized surface fluxes

4.3.1 Annually integrated fluxes

In Figs. 7 and 8, the optimized fluxes are presented after aggregation over one year and different land and ocean regions. For reference, the regions are defined as global $0.5^\circ \times 0.5^\circ$ masks in the Supplement. The error bars are 1σ posterior errors. The rightmost group of bars in Fig. 8 denote the global budget of CO_2. The difference between the global budgets predicted by a surface-only inversion and a joint surface + GOSAT inversion corresponds to a difference of 0.5 ppm in the global average CO_2 mixing ratio. From an 18 month inversion it is not possible to constrain the global growth rate to a higher accuracy, and future inversions over longer periods will be able to separate the trend from interannual variability. Of the additional 1 PgC predicted by the joint

ACPD
13, 4535–4600, 2013

inversion, 90 % lies above 850 hPa, which is consistent with the fact that in the surface layer both the surface-only inversion and the joint inversion are consistent with surface stations.

Figure 9 shows the posterior correlation matrix between the different emissions shown in Figs. 7 and 8, for the inversion assimilating both surface CO_2 and GOSAT X_{CO_2} measurements. For geographically disjoint regions, a near-zero correlation would imply that the emissions from those regions can be independently constrained by the observations, whereas a high negative correlation would indicate a compensatory mechanism. To conclude that optimized emissions over a certain region during a certain period are robust – as opposed to artefacts of inversion – there must be significant uncertainty reduction, i.e. in Figs. 7 and 8 the posterior error bar must be smaller than the prior error bar. Moreover, the correction to prior emission over that region must not be strongly negatively correlated to the correction over a geographically disjoint region in Fig. 9. This would mean, for example, that although the global 2.3 PgC sink between 1 September 2009 and 1 Septmber 2010 is a robust conclusion from a joint GOSAT + surface CO_2 inversion, its partitioning between a 2 PgC land source and a 4.3 PgC ocean sink is not; a correlation of −0.97 between global land and global ocean in Fig. 9 points to an inability of the inversion to independently constrain the emissions from those two regions. Similarly, although tropical Asia does not have a significant correlation with any other TRANSCOM region in Fig. 9, it shows only 15 % uncertainty reduction in a joint inversion, limiting the trustworthiness of the estimated 0.2 PgC source.

4.3.2 Seasonal variation of CO_2 flux

We group the optimized flux over 18 months for each region into blocks of three months, which splits a year into summer, fall, winter and spring. Figure 10 (top row) shows that in the northern extra-tropics, assimilation of GOSAT data leads to a slightly higher uptake in the NH summer of 2009 (JJA '09) and slightly higher outgassing in the NH winter of 2009–2010 (DJF '09). The strengthening of uptake and outgassing are independent events and not compensations for each other to maintain a consistent annual

ACPD
13, 4535–4600, 2013

budget, since they have no posterior correlation (Fig. 11, left). Since CONTRAIL data in Sect. 4.2.1 do not support this enhancement, it could be an artefact of transport error as opposed to a real signal. Whether this is specific to the seasonal cycle in 2009 or whether this is a more generic feature can only be answered in the future with multi-year GOSAT inversions.

Figure 10 (middle row) shows that in the tropics, assimilating GOSAT X_{CO_2} results in a CO_2 drawdown in the NH summer of 2009 due to increased uptake by the tropical land, and increased outgassing from the tropical land in the NH spring of 2010 leads to a CO_2 increase. The two events are independent (Fig. 11, center), and it is likely that the increased outgassing in MAM 2010 is a genuine surface flux signal, since it is also visible in CONTRAIL samples over the tropics (Fig. 5, right).

Assimilating GOSAT X_{CO_2} increases the seasonal cycle amplitude of the CO_2 flux from the southern extra-tropics, as seen in Fig. 10 (bottom row). In SH spring (SON '09 and SON '10) GOSAT X_{CO_2} points to an outgassing of CO_2 from the land, while in SH summer (DJF '09) GOSAT X_{CO_2} indicates a deeper oceanic sink of CO_2 than what is consistent with surface measurements. This leads to a net amplification of the CO_2 seasonal cycle. This enhancement is seen neither by the southern temperate TCCON stations such as Wollongong (Fig. 6) nor by surface stations in those latitudes such as Crozet Island (Fig. 3). Since this enhanced seasonality is present in the GOSAT X_{CO_2} as evidenced by its comparison with TCCON X_{CO_2} at Wollongong in Fig. 6 (center), there is likely a retrieval artefact over the southern temperate latitudes that leads to a spurious strengthening of the CO_2 seasonal cycle in the south. Alternatively, there could also be a retrieval artefact over oceans, which would alias into the X_{CO_2} seasonal cycle over the southern temperate latitudes owing to the high percentage of ocean cover there and their seasonally varying satellite coverage. Indeed, we will see in Sect. 4.5 that allowing for a global land-sea bias in the assimilated X_{CO_2} and estimating it during the inversion gets rid of part of the spurious seasonal cycle enhancement seen in Fig. 4.

ACPD
13, 4535–4600, 2013

4.4 Robustness of optimized fluxes

As mentioned in Sect. 3.4, we perform our inversion with three slightly modified configurations to test the robustness of optimized fluxes. The first modification involves the vertical resolution. For all the inversions presented so far, we have used the TM5 transport model with 25 vertical layers. The meteorological fields driving the model, from the ECMWF ERA Interim dataset, are however available at the finer resolution of 60 vertical layers. It is therefore possible to simulate atmospheric transport by TM5 over 60 vertical layers. We expect the 60 layer model to better simulate the vertical CO_2 profile, to which GOSAT X_{CO_2} is sensitive. Therefore, at least for inversions assimilating GOSAT data, the 60 layer model should yield flux estimates closer to the "truth" than the coarser, 25 layer model. To test the impact of changing the vertical resolution of the transport model on the optimized fluxes, we assimilated the same data sets (surface layer and GOSAT) in inversions using TM5 with 25 and 60 vertical layers.

Yearly aggregated fluxes from both the 25 layer and the 60 layer inversions are presented for a few large regions in Fig. 12. As we can see, changing the vertical resolution from the coarse 25 layers to the maximum possible 60 layers does not change the optimized fluxes significantly, implying that TM5 with 25 vertical layers is as good as TM5 at the full vertical resolution for ingesting both surface and satellite data. It should be noted that we performed this test using inversions based on an earlier version of the RemoTeC X_{CO_2} product for both vertical resolutions, hence the differences between aggregated fluxes in Figs. 12 and 8. Since the result of the test was that the vertical model resolution makes only negligible differences to the optimized flux, we did not perform 60-layer inversions with the RemoTeC X_{CO_2} data used for the results presented in Sect. 4.3.

The second modification involves the horizontal resolution, where we run our transport model at global $3^\circ \times 2^\circ$ resolution. Changing the horizontal resolution changes the resolution of synoptic weather patterns, the time scales for horizontal diffusion and vertical convection and thereby the interhemispheric transport time, and the

ACPD
13, 4535–4600, 2013

representability of local fluctuations in the CO_2 concentration. It would not be unreasonable, therefore, to expect very different optimized fluxes (compared to the $6^\circ \times 4^\circ$ transport model) given the same set of assimilated observations. In practice, however, the effect of running our inversions at a different lateral resolution did not turn out to be large, as seen in Fig. 13. Over some regions such as the northern extra-tropics, changing the horizontal resolution changed the estimate of optimized fluxes, although at the level of the posterior error estimates the changes are not significant. Over other regions such as the tropics, refining the lateral model resolution did not change the flux estimates.

The third modification involves changing the assimilated meteorological dataset driving the TM5 transport model. Using ECMWF operational forecasts instead of Era Interim reanalyzed meteorological data is equivalent to using a different realization of atmospheric transport, and we would in general expect estimated fluxes to differ, especially if one of the meteorological datasets were significantly different from the "truth". However, the effect of changing the driving meteo did not prove to be large, as seen in Fig. 14. Over all regions, the estimated fluxes from the two realizations of transport were within $1 - \sigma$ of each other.

4.5 Optimizing a land-ocean bias

Figures 4 and 6 show that assimilating GOSAT X_{CO_2} leads to an overestimation of the seasonal cycle in the southern extra-tropics. We also know that the land-ocean partitioning of the global carbon sink in Fig. 8 is not realistic, because it shows a large net land source of carbon, contrary to the present understanding of the terrestrial carbon cycle. We suspect that the two problems have a common origin, viz. problematic X_{CO_2} retrievals over oceans. Since most of the southern extra-tropics is covered by oceans, which has a seasonally varying coverage from GOSAT due to the strict requirements of the glint geometry, a systematic land-sea bias in GOSAT X_{CO_2} would alias into the seasonal cycle of the southern extra-tropics. To investigate the plausiblity of a land-sea bias in our GOSAT X_{CO_2} retrievals, we introduce two bias parameters, b_{land} and b_{ocean},

ACPD
13, 4535–4600, 2013

with the interpretation that retrieved values of X_{CO_2} are off from the "true" values of X_{CO_2} by b_{land} and b_{ocean} over land and ocean, respectively:

$$X_{CO_2}(land,true) = X_{CO_2}(land,retrieved) + b_{land}$$
$$X_{CO_2}(ocean,true) = X_{CO_2}(ocean,retrieved) + b_{ocean} \quad (7)$$

We then try to find the optimal values of $b_{land,ocean}$ by an inversion assimilating GOSAT and surface layer CO_2 data. We start with prior values of 0 ppm for both, and since land pixels are better calibrated than ocean pixels owing to TCCON stations on land, we assign prior errors of $\sigma(b_{land}) = 1$ ppm and $\sigma(b_{ocean}) = 2$ ppm. Even though we're primarily interested in a land-ocean bias, we optimize not one but two parameters b_{land} and b_{ocean} since a single degree of freedom would imply that the overall level is perfectly constrained, which is not the case. At the same time, the offsets over land and ocean should not be completely independent, so we constrain $\boldsymbol{b}$ to have 1.4 degrees of freedom by assigning a prior correlation of $corr(b_{land}, b_{ocean}) = -0.65$. After assimilating GOSAT and surface CO_2 data, the optimal values of the bias parameters are $b_{land} = -0.14 \pm 0.04$ ppm and $b_{ocean} = 0.79 \pm 0.04$ ppm. As seen in Figs. 15 and 16, with this simple bias correction, the optimized fluxes (labeled "(BC)" in subsequent figures) have much more realistic land-ocean partitioning. The global land is now a $0.6 \pm 0.4\,PgC\,yr^{-1}$ sink instead of a net carbon source, and the global ocean is now a $1.7 \pm 0.4\,PgC\,yr^{-1}$ sink, which is very similar to a surface-only inversion. The tropical ocean becomes a $0.8 \pm 0.2\,PgC\,yr^{-1}$ source, and the poleward carbon flux, i.e. the carbon sourcing in the tropics and sinking in the extra-tropics, is increased compared to a surface-only inversion.

Optimizing for a land-ocean bias in GOSAT X_{CO_2} in our data assimilation also reduces the enhancement of the seasonal cycle in the southern extra-tropics discussed before. Figure 17 shows that if we account for a possible land-ocean bias in assimilated X_{CO_2}, the posterior CO_2 time series at the surface in the southern extra-tropics displays a higher concentration of CO_2 in the NH winter of 2009–2010. This reduces the spurious enhancement of the seasonal cycle at these latitudes as mentioned before. We

ACPD
13, 4535–4600, 2013

conclude that small biases in our ocean retrievals, coupled with the seasonally varying coverage of GOSAT ocean pixels, results in the spurious enhancement of the southern extra-tropical CO_2 seasonal cycle. Ocean pixels have a much higher signal to noise ratio due to the high surface reflectivity in sunglint geometry, so in principle they could be more accurate than land pixels. Therefore, we are currently working on improving our ocean X_{CO_2} retrievals to eliminate the remaining biases. Pending further improvements to our ocean retrievals, we consider a joint inversion of surface and satellite data along with the optimization of two bias parameters from Eq. (7) as the most reliable method for assimilating RemoTeC X_{CO_2} in a source-sink inversion. Below, we briefly summarize optimized emissions from this joint inversion where the numbers quoted hold up to scrutiny both in terms of uncertainty reduction and posterior correlation, as mentioned in Sect. 4.3.1.

A surface-only inversion changes the 0.4 ± 0.5 PgC North American (prior) source into a 0.4 ± 0.2 PgC sink. Adding GOSAT X_{CO_2} strengthens this sink to 1.0 ± 0.1 PgC. Europe goes from a 0.3 ± 0.4 PgC prior source to a 0.3 ± 0.3 PgC sink in a surface-only inversion, with the addition of GOSAT strengthening the sink to 1.3 ± 0.2 PgC, although part of it is to compensate the sourcing from the North Atlantic. South America, a 0.5 ± 0.5 PgC sink in the prior, is slightly weakened by the surface inversion to 0.4 ± 0.4 PgC, and assimilating GOSAT X_{CO_2} turns it almost carbon neutral, a small 0.1 ± 0.2 PgC source. The Eurasian boreal region, which was a 1.1 ± 0.3 PgC sink according to a surface-only inversion, is considerably weakened to 0.3 ± 0.2 PgC on assimilating GOSAT. The Eurasian temperate region is turned from a 0.1 ± 0.2 PgC sink (surface-only) to a 0.3 ± 0.2 PgC source (surface + GOSAT), turning Asia into a net source of 0.3 ± 0.3 PgC from a surface-only estimate of 1 ± 0.4 PgC sink. Part of this, however, could be a compensatory effect to offset the enhanced sinking in the North Pacific. Overall, the prior 0.3 ± 0.7 PgC sourcing from the tropics is strengthened by a surface inversion to 0.5 ± 0.4 PgC, which is further enhanced to a 2.1 ± 0.2 PgC source on addition of GOSAT X_{CO_2}. The land-ocean partitioning of this source (1.3 ± 0.2 PgC from land and 0.8 ± 0.2 from ocean) is less trustworthy owing to a -0.57 posterior

ACPD
13, 4535–4600, 2013

correlation between tropical land and tropical ocean. A part of this additional CO_2 is taken up by the northern extra-tropical sink (2.1 ± 0.3 PgC for a surface-only inversion compared to 2.9 ± 0.1 PgC for a surface + GOSAT inversion), and the rest contributes to the weaking of the global sink from 3.4 ± 0.2 PgC (surface only) to 2.3 ± 0.1 PgC (surface + GOSAT).

5 Discussion

In Sect. 4 we presented the results of our source-sink inversions between 1 June 2009 and 1 December 2010 using both GOSAT X_{CO_2} and surface measurements of CO_2. We saw in Sect. 4.1 that when we optimized surface CO_2 fluxes against only GOSAT X_{CO_2}, we could reproduce the CO_2 time series at surface stations in the tropics and northern extra-tropics. In the northern extra-tropics, assimilating only GOSAT X_{CO_2} corrects the underestimated summer uptake of the CASA prior fluxes, and also improves the phasing of the seasonal cycle. Surface fluxes optimized against GOSAT measurements could also reproduce the X_{CO_2} time series at TCCON stations situated in these latitudes, evidenced in Fig. 6 at Lamont and several European stations. We stress that this is the first definite demonstation that X_{CO_2} measurements from GOSAT and similar future satellite missions can quantify the carbon cycle, a result that bodes well for future remote sensing missions. However, our results also point to remaining problems in RemoTeC retrievals over the southern extra-tropics. Inversions assimilating GOSAT X_{CO_2} show enhanced seasonal cycles not seen in other independent atmospheric measurements. Corresponding inversion-derived seasonal emission adjustments are found over the southern extra-tropics, such as CO_2 emissions from the southern extra-tropical land during SON '09 and SON '10, and enhanced CO_2 uptake by the southern extra-tropical ocean in DJF '09 (Fig. 10, bottom row). The effect of this enhancement is visible in the simulated surface layer CO_2 time series at surface stations in the southern extra-tropical latitudes, such as Crozet Island in Fig. 3. This enhancement is also visible in simulated TCCON time series from those latitudes, such as at Wollongong in Fig. 6.

ACPD
13, 4535–4600, 2013

Since neither the surface stations nor TCCON see this enhanced seasonal cycle, we suspect that this enhancement is a spurious effect of retrieval artefacts as opposed to a true surface flux signal. In fact, co-located GOSAT data over Wollongong (Fig. 6, center), compared to TCCON X_{CO_2}, show a higher bias in SON '09 and SON '10 as opposed to MAM '10, indicating that this enhancement could be a direct effect of the X_{CO_2} data ingested instead of a transport model error. To be certain of this conclusion, we need to compare GOSAT X_{CO_2} in this latitude band with ground-based X_{CO_2} measurements from several locations. Unfortunately, the only other TCCON station in the southern extra-tropics, Lauder, has a data gap during MAM '10.

Following the method of Conway et al. (1994), the increase in the global average CO_2 mixing ratio derived by NOAA between 1 September 2009 and 1 September 2010 is 2.72 ppm (data downloaded from ftp://ftp.cmdl.noaa.gov/ccg/co2/trends/co2_mm_gl.txt). The global CO_2 emission over that period predicted by our inversions (Fig. 8) corresponds to increases of 2.4 ± 0.1 ppm (surface data only), 2.99 ± 0.04 ppm (GOSAT only) and 2.86 ± 0.04 ppm (joint assimilation). All three estimates are in line with the NOAA estimate, and the remaining discrepancies can be explained by the fact that while the NOAA estimate is the result of a multi-year trend analysis, we have only optimized the flux for 18 months, and are thus significantly affected by interannual variability. The trend estimation method of Thoning et al. (1989) used by Conway et al. (1994) cannot be used in our case since the data record is too short. In the future, with multi-year GOSAT inversions, the comparison with the NOAA flask-derived estimate of CO_2 growth rate could prove to be more insightful.

Although the global CO_2 budget in Fig. 8 is consistent with independent estimates such as the one from NOAA, the land-ocean partitioning of the global total flux is less reliable, in particular the global land biosphere turning out to be a net source of carbon is not believable. We suspect that this erroneous partitioning is due to a retrieval problem over the ocean, since land retrievals are rather well calibrated against TCCON measurements. We show that optimizing for a global bias between land and ocean X_{CO_2} retrievals not only makes the partitioning more realistic, it also reduces

ACPD
13, 4535–4600, 2013

the spurious enhancement of the seasonal cycle seen in the southern extra-tropics. The performance of a joint inversion which optimizes a global land-sea bias in X_{CO_2} is good enough for us to consider it as our standard joint inversion.

We would like to stress here that a total land-ocean bias of 0.93 ppm was enough to induce the dramatic changes in land-ocean partitioning of the fluxes seen in Fig. 16. This emphasises the stringent accuracy requirements on satellite X_{CO_2} to be used for source-sink inversions of CO_2. A 0.93 ppm bias between land and ocean pixels is not something that can be constrained by the present GOSAT X_{CO_2} validation technique of comparison to X_{CO_2} from the TCCON network, but such a bias is enough to significantly change the picture of the global carbon cycle arrived at through an atmospheric inversion. Though the TCCON network is in theory accurate enough detect this 0.93 ppm bias, the current lack of marine TCCON instruments makes this detection impossible.

We would also like to caution that studies assimilating any total column data in the near infrared – be it TCCON, GOSAT or some other satellite – could in principle suffer from fair weather bias, since only X_{CO_2} retrievals from scenes taken during clear sky and low aerosol conditions are assimilated. The impact of this would be felt in the tropics due to intermittent cloud cover, and in the northern high latitudes in NH winter for similar reasons. Areas of high aerosol content, such as downwind of the Sahara and the Gobi deserts, could also be under-sampled, leading to biases.

Based on surface CO_2 time series and source-sink inversions assimilating surface CO_2 observations, previous studies have estimated the northern extra-tropics to be a strong sink of carbon, whereas the tropics have been estimated to be a strong source (Gurney et al., 2002; Gurney, 2004; Tans et al., 1990). The magnitude of this carbon flux, however, has been the subject of some debate. Stephens et al. (2007) showed that global flux scenarios that had weaker poleward carbon fluxes produced atmospheric CO_2 fields more consistent with aircraft measurements of CO_2. We could thus expect that incorporating CO_2 measurements from aircrafts in a source-sink analysis would weaken the strengths of the tropical source and extra-tropical sink, compared to inversions assimilating only surface CO_2 data. In this study, we find that assimilating

ACPD
13, 4535–4600, 2013

GOSAT X_{CO_2} in addition to surface CO_2 data strengthens the poleward carbon flux, i.e. the tropics become a larger source and the extra-tropics become a deeper sink. As shown in Fig. 16, in a surface data-only inversion, the tropics are a net source of $0.5 \pm 0.4\,PgC\,yr^{-1}$, whereas the northern extra-tropics are a net sink of $2 \pm 0.3\,PgC\,yr^{-1}$. After assimilating GOSAT X_{CO_2}, the tropics source $2.1 \pm 0.2\,PgC\,yr^{-1}$, and the northern extra-Tropics sink $2.9 \pm 0.1\,PgC\,yr^{-1}$. We believe this enhancement of the poleward carbon flux to be a robust result within our inversion framework, since it survives all our sensitivity tests mentioned in Sect. 4.4. We note, however, that Stephens et al. (2007) found a lage spread in the estimate of the northern extra-tropical sink between different inversions due to differences in vertical transport, and we need to assess the accuracy of vertical transport in TM5 by comparing modeled CO_2 with aircraft profiles to have more confidence in our result. Further, this enhancement of the tropical source and extra-tropical sink, even if robust, could be a feature of the period presented in Sect. 4.3.1, and in the future we plan to explore this question further with multi-year inversions.

The majority of the northern extra-tropical carbon sinking mentioned by Tans et al. (1990) and others happens in the forests and grasslands of N America and boreal Eurasia. With globally increasing CO_2 levels and the changing climate, it is an open question whether these sinks are becoming more or less powerful. Existing biosphere models underestimate the size of these sinks (Messerschmidt et al., 2012; Yang et al., 2007), as do some inversions using only surface CO_2 measurements (Basu et al., 2011). Therefore it is important to impose additional observational constraints to estimate these sinks more accurately, and then to monitor the evolution of these sinks over time. Our estimate of the N American carbon sink ($1.0 \pm 0.1\,PgC\,yr^{-1}$) is higher when we assimilate GOSAT X_{CO_2} and surface CO_2 as opposed to when we assimilate only surface CO_2 ($0.4 \pm 0.2\,PgC\,yr^{-1}$). We believe this result to be robust within our inversion framework and not an artefact of inversion since Fig. 9 shows no appreciable posterior correlation between N America and other regions. For the same reason, the weakening of the Eurasian boreal sink ($-1.1 \pm 0.3\,PgC\,yr^{-1}$ for a surface-only inversion

ACPD
13, 4535–4600, 2013

compared to $0.3 \pm 0.2\,\mathrm{PgC\,yr^{-1}}$ when GOSAT data are included) could be a robust result as well. An enhanced uptake over N America and a reduced uptake over Eurasia fits the observed scenario that the TCCON time series at N American sites such as Lamont (Fig. 6) show a summer uptake beyond that predicted by surface data, whereas those over European sites do not. CONTRAIL samples over this latitude band, which are more indicative of the uptake over the entire northern temperate latitudes rather than individual continents, also do not show an enhanced uptake (Fig. 5). Whether these are specific to the summer of 2010 or systematic remains to be seen from future multi-year inversions with GOSAT data.

It is interesting to compare the flux estimates we obtain from a joint inversion with bias optimization for the period 1 September 2009 to 1 September 2010 with other inversion products. There are only a few top-down estimates for this period, and we choose two for comparison, (a) the recently-released CarbonTracker 2011 (CT2011), and (b) an atmospheric inversion assimilating TCCON X_{CO_2} by Chevallier et al. (2011).

Figure 18 compares CT2011 fluxes with aggregated fluxes from our surface data-only and joint inversions for the TRANSCOM regions and global land and sea. We assimilate the same surface data set as CT2011 and use the same tracer transport model (TM5), and therefore we could expect our surface-data only inversion to correspond closely to CT2011. It turns out that aggregated fluxes from our surface-only inversion and CT2011 fluxes are within 1σ of each other, except over parts of the Pacific. Comparing CT2011 fluxes to our standard product, i.e. a joint inversion with optimized land-sea bias correction, turns up more significant differences. At the large scale, the most significant difference between CT2011 and our bias-optimized joint inversion is that our inversion predicts a significantly smaller land sink (0.6 ± 0.4 PgC) compared to CT2011 (1.9 PgC). The difference does not stem from a single region, but is spread over multiple areas. The North American and European sinks are stronger in our inversion, but the Eurasian boreal sink is weaker. The Eurasian temperate sink seen in CT2011 is a source for us, and the African source of CT2011 is enhanced significantly. We caution that GOSAT X_{CO_2} over large parts of Africa and the Eurasian temperate

ACPD
13, 4535–4600, 2013

region cannot be calibrated against any TCCON measurements, while the Eurasian boreal region has seasonal coverage and is therefore subject to a seasonal sampling bias. Hence the flux estimates over these three regions from our joint inversion should be interpreted with caution.

The global oceanic sink is the same for both CT2011 and our joint inversion, but the distribution is not identical. The Southern ocean is a stronger sink in our joint inversion, as are the north Pacific temperate and the south Atlantic temperate. On the other hand, the south Pacific temperate is a weaker sink. The north Atlantic temperate is a source in our inversion, which does not agree with our existing knowledge of the oceanic carbon cycle, and therefore points to remaining retrieval issues not addressed by our simple bias correction scheme.

According to Chevallier et al. (2011), TCCON X_{CO_2} mostly constrains terrestrial sources and sinks, so in (Chevallier et al., 2011) they presented aggregated annual fluxes over the 11 TRANSCOM land regions. We compare our estimates between 1 September 2009 and 1 September 2010 with their estimates over the same period after deducting fossil fuel fluxes in Fig. 19 (Chevallier, personal communication, 2012). The global land sink from our inversion is weaker compared to Chevallier et al. (2011), just as it was weaker compared to CT2011. The differences over land are most striking in the Americas. We predict a much stronger carbon sink over North America and a small carbon source over South America, compared to a net South American sink in (Chevallier et al., 2011). Interestingly, the posterior atmospheric CO_2 fields from both inversions are consistent with TCCON X_{CO_2} measurements over North America, because Chevallier et al. (2011) assimilated TCCON X_{CO_2} while we assimilated GOSAT X_{CO_2} which were validated against TCCON X_{CO_2}. This suggests that at present, different X_{CO_2} measurements consistent with the same set of TCCON X_{CO_2} can yield dramatically different posterior flux distributions, even over regions such as North America, which has several TCCON stations.

ACPD
13, 4535–4600, 2013

6 Conclusions

In this manuscript we have presented optimized global source-sink estimates of CO_2 using the RemoTeC retrieval of GOSAT xCO over eighteen months from 1 June 2009 to 1 December 2010. We have compared the flux estimates with a more conventional 4DVAR inversion using data only from surface-layer CO_2 measurements. We have shown that GOSAT X_{CO_2} is consistent with surface stations in the tropics and northern extra-tropics, whereas in the southern extra-tropics it has a higher seasonal cycle compared to surface stations. We believe that this enhanced seasonal cycle is due to a retrieval artefact over the oceans. We show that optimizing a global bias between land and ocean retrievals of GOSAT X_{CO_2} points to a 0.93 ppm remaining bias between them, and demonstrate that this sub-ppm bias significantly changes the picture of the terrestrial carbon cycle we can derive by assimilating GOSAT X_{CO_2}.

We have shown that the global budget is well-constrained by GOSAT X_{CO_2} to yield a global CO_2 growth rate consistent with the NOAA estimate using the method of Conway et al. (1994), although the land-sea partitioning of the global flux remains problematic. We find that both the tropical source and the extra-tropical sink of carbon estimated in earlier works (Gurney et al., 2002; Gurney, 2004; Tans et al., 1990) are strengthened when we include GOSAT X_{CO_2} in our inversion. This is a robust result within our inversion framework, although it contrasts with earlier findings by Stephens et al. (2007). We also find that the N American carbon sink is slightly stronger than predicted by a surface data-only inversion, although N America is well covered by the surface measurement network and the effect of introducing GOSAT data is small.

We caution that these are results using one retrieval (RemoTeC) for slightly more than one year, and the RemoTeC L2 data product is under constant development. More importantly, our estimate of transport uncertainty is likely to be too small since we've used a single transport model. Although we did perform several sensitivity tests as shown in Sect. 4.4, it remains to be seen whether our conclusions hold up when a different – possibly improved – retrieval data set is assimilated or when a different

ACPD
13, 4535–4600, 2013

transport model is used, and if the features we observe are specific to our inversion period or if they recur every year. As the GOSAT X_{CO_2} dataset is extended through 2011 and 2012, we hope to address those questions in our future work with multiple GOSAT X_{CO_2} retrievals and over multiple years.

Supplementary material related to this article is available online at: http://www.atmos-chem-phys-discuss.net/13/4535/2013/acpd-13-4535-2013-supplement.zip.

Acknowledgements. We thank Frédéric Chevallier for providing us with fossil fuel adjusted flux aggregates from (Chevallier et al., 2011) and the CONTRAIL PIs Toshinobu Machida, Hidekazu Matsueda and Yousuke Sawa for providing the CONTRAIL data. André Butz was supported by the Emmy-Noether program of the Deutsche Forschungsgemeinschaft (DFG) through grant BU2599/1-1 (RemoteC). Sourish Basu was supported by the Gebruikersondersteuning ruimteonderzoek program of the Nederlandse organisatie voor Wetenschappelijk Onderzoek (NWO) through project ALW-GO-AO/08-10. Computer resources for model runs was provided by SARA through NCF project number SH-026-12. Access to GOSAT data was granted through the 2nd GOSAT research announcement jointly issued by JAXA, NIES and MOE. TCCON data were obtained from the TCCON Data Archive, operated by the California Institute of Technology from the website at http://tccon.ipac.caltech.edu/. US funding for TCCON comes from the Terrestrial Ecology Program of the National Aeronautics and Space Administration (NASA), grant number NNX11AG01G, the Orbiting Carbon Observatory Program, the Atmospheric CO2 Observations from Space (ACOS) Program and the DOE/ARM Program. Some of the research described in this paper was performed at the Jet Propulsion Laboratory, California Institute of Technology, under a contract with NASA. We acknowledge funding to support the Wollongong TCCON instrument from the Australian Research Council, Projects LE0668470, DP0879468, DP110103118 and LP0562346. We acknowledge financial support of the Bialystok and Orléans TCCON sites from the Senate of Bremen and EU projects IMECC and GEOmon as well as maintenance and logistical work provided by AeroMeteo Service (Bialystok) and the RAMCES team at LSCE (Gif-sur-Yvette, France).

ACPD
13, 4535–4600, 2013

References

Basu, S., Houweling, S., Peters, W., Sweeney, C., Machida, T., Maksyutov, S., Patra, P. K., Saito, R., Chevallier, F., Niwa, Y., Matsueda, H., and Sawa, Y.: The seasonal cycle amplitude of total column CO_2: factors behind the model-observation mismatch, J. Geophys. Res., 116, D23306, doi:10.1029/2011JD016124, 2011. 4539, 4567

Beardsmode, D. J. and Pearman, G. I.: Atmospheric carbon dioxide measurements in the Australian region: data from surface observatories, Tellus B, 39, 42–66, doi:10.1111/j.1600-0889.1987.tb00269.x, 1987. 4536

Blasing, T. J., Broniak, C. T., and Marland, G.: Estimates of monthly carbon dioxide emissions and associated δ13C values from fossil-fuel consumption in the U. S. A. In Trends: A Compendium of Data on Global Change, Tech. rep., Carbon Dioxide Information Analysis Center, Oak Ridge National Laboratory, US Department of Energy, Oak Ridge, Tennessee, doi:10.3334/CDIAC/ffe.001, available at: http://cdiac.ornl.gov/trends/emis_mon/emis_mon_co2.html (last access: November 2012), 2005. 4546

Boden, T. A., Marland, G., and Andres, R. J.: Global, Regional, and National Fossil-Fuel CO_2 Emissions, Tech. rep., Oak Ridge, Tennessee, doi:10.3334/CDIAC/00001_V2010, available at: http://cdiac.ornl.gov/trends/emis/overview_2007, 2010. 4546

Boesch, H., Baker, D., Connor, B., Crisp, D., and Miller, C.: Global characterization of CO_2 column retrievals from shortwave-infrared satellite observations of the orbiting carbon observatory-2 mission, Remote Sensing, 3, 270–304, doi:10.3390/rs3020270, 2011. 4537

Buchwitz, M., Schneising, O., Burrows, J. P., Bovensmann, H., Reuter, M., and Notholt, J.: First direct observation of the atmospheric CO_2 year-to-year increase from space, Atmos. Chem. Phys., 7, 4249–4256, doi:10.5194/acp-7-4249-2007, 2007. 4537

Butz, A., Hasekamp, O. P., Frankenberg, C., and Aben, I.: Retrievals of atmospheric CO_2 from simulated space-borne measurements of backscattered near-infrared sunlight: accounting for aerosol effects, Appl. Optics, 48, 3322–3336, doi:10.1364/AO.48.003322, 2009. 4542

Butz, A., Hasekamp, O. P., Frankenberg, C., Vidot, J., and Aben, I.: CH_4 retrievals from space-based solar backscatter measurements: performance evaluation against simulated aerosol and cirrus loaded scenes, J. Geophys. Res., 115, D24302, doi:10.1029/2010JD014514, 2010. 4542

Butz, A., Guerlet, S., Hasekamp, O., Schepers, D., Galli, A., Aben, I., Frankenberg, C., Hartmann, J.-M., Tran, H., Kuze, A., Keppel-Aleks, G., Toon, G., Wunch, D., Wennberg, P.,

ACPD
13, 4535–4600, 2013

Deutscher, N., Griffith, D., Macatangay, R., Messerschmidt, J., Notholt, J., and Warneke, T.: Toward accurate CO_2 and CH_4 observations from GOSAT, Geophys. Res. Lett., 38, L14812–L14812, doi:10.1029/2011GL047888, 2011. 4538, 4542

Butz, A., Galli, A., Hasekamp, O., Landgraf, J., Tol, P., and Aben, I.: TROPOMI aboard Sentinel-5 precursor: prospective performance of CH_4 retrievals for aerosol and cirrus loaded atmospheres, Remote Sens. Environ., 120, 267–276, doi:10.1016/j.rse.2011.05.030, 2012. 4542

CarbonTracker: CarbonTracker 2011 – ESRL Global Monitoring Division, http://www.esrl.noaa.gov/gmd/ccgg/carbontracker/documentation.html, 2012. 4546

Chahine, M. T., Pagano, T. S., Aumann, H. H., Atlas, R., Barnet, C., Blaisdell, J., Chen, L., Divakarla, M., Fetzer, E. J., Goldberg, M., Gautier, C., Granger, S., Hannon, S., Irion, F. W., Kakar, R., Kalnay, E., Lambrigtsen, B. H., Lee, S.-Y., Le Marshall, J., McMillan, W. W., McMillin, L., Olsen, E. T., Revercomb, H., Rosenkranz, P., Smith, W. L., Staelin, D., Strow, L. L., Susskind, J., Tobin, D., Wolf, W., and Zhou, L.: AIRS: improving weather forecasting and providing new data on greenhouse gases, B. Am. Meteorol. Soc., 87, 911–926, doi:10.1175/BAMS-87-7-911, 2006. 4537

Chédin, A., Serrar, S., Scott, N. A., Crevoisier, C., and Armante, R.: First global measurement of midtropospheric CO_2 from NOAA polar satellites: tropical zone, J. Geophys. Res., 108, 4581, doi:10.1029/2003JD003439, 2003. 4537

Chevallier, F.: Impact of correlated observation errors on inverted CO_2 surface fluxes from OCO measurements, Geophys. Res. Lett., 34, L24804, doi:10.1029/2007GL030463, 2007. 4543

Chevallier, F.: Personal communication, 2012. 4569

Chevallier, F., Fisher, M., Peylin, P., Serrar, S., Bousquet, P., Bréon, F.-M., Chédin, A., and Ciais, P.: Inferring CO2 sources and sinks from satellite observations: method and application to TOVS data, J. Geophys. Res., 110, D24309, doi:10.1029/2005JD006390, 2005. 4538, 4543

Chevallier, F., Bréon, F.-M., and Rayner, P. J.: Contribution of the orbiting carbon observatory to the estimation of CO_2 sources and sinks: theoretical study in a variational data assimilation framework, J. Geophys. Res., 112, D09307, doi:10.1029/2006JD007375, 2007. 4537

Chevallier, F., Engelen, R. J., Carouge, C., Conway, T. J., Peylin, P., Pickett-Heaps, C., Ramonet, M., Rayner, P. J., and Xueref-Remy, I.: AIRS-based versus flask-based estimation of carbon surface fluxes, J. Geophys. Res., 114, D20303, doi:10.1029/2009JD012311, 2009. 4538, 4539

ACPD
13, 4535–4600, 2013

Chevallier, F., Ciais, P., Conway, T. J., Aalto, T., Anderson, B. E., Bousquet, P., Brunke, E. G., Ciattaglia, L., Esaki, Y., Fröhlich, M., Gomez, A., Gomez-Pelaez, A. J., Haszpra, L., Krummel, P. B., Langenfelds, R. L., Leuenberger, M., Machida, T., Maignan, F., Matsueda, H., Morguí, J. A., Mukai, H., Nakazawa, T., Peylin, P., Ramonet, M., Rivier, L., Sawa, Y., Schmidt, M., Steele, L. P., Vay, S. A., Vermeulen, A. T., Wofsy, S., and Worthy, D.: CO_2 surface fluxes at grid point scale estimated from a global 21 year reanalysis of atmospheric measurements, J. Geophys. Res., 115, D21307, doi:10.1029/2010JD013887, 2010. 4536

Chevallier, F., Deutscher, N. M., Conway, T. J., Ciais, P., Ciattaglia, L., Dohe, S., Fröhlich, M., Gomez-Pelaez, A. J., Griffith, D., Hase, F., Haszpra, L., Krummel, P., Kyrö, E., Labuschagne, C., Langenfelds, R., Machida, T., Maignan, F., Matsueda, H., Morino, I., Notholt, J., Ramonet, M., Sawa, Y., Schmidt, M., Sherlock, V., Steele, P., Strong, K., Sussmann, R., Wennberg, P., Wofsy, S., Worthy, D., Wunch, D., and Zimnoch, M.: Global CO_2 fluxes inferred from surface air-sample measurements and from TCCON retrievals of the CO_2 total column, Geophys. Res. Lett., 38, L24810, doi:10.1029/2011GL049899, 2011. 4568, 4569, 4571, 4600

Conway, T. J., Tans, P. P., Waterman, L. S., Thoning, K. W., Kitzis, D. R., Masarie, K. A., and Zhang, N.: Evidence for interannual variability of the carbon cycle from the national oceanic and atmospheric administration/climate monitoring and diagnostics laboratory global air sampling network, J. Geophys. Res., 99, 22831–22855, doi:10.1029/94JD01951, 1994. 4565, 4570

Courtier, P., Thépaut, J.-N., and Hollingsworth, A.: A strategy for operational implementation of 4D-Var, using an incremental approach, Q. J. Roy. Meteor. Soc., 120, 1367–1387, doi:10.1002/qj.49712051912, 1994. 4551

Crevoisier, C., Chédin, A., Matsueda, H., Machida, T., Armante, R., and Scott, N. A.: First year of upper tropospheric integrated content of CO_2 from IASI hyperspectral infrared observations, Atmos. Chem. Phys., 9, 4797–4810, doi:10.5194/acp-9-4797-2009, 2009. 4537

Dobbs, M., Dobler, J., Moore, B., Browell, E., Harrison, F. W., and Snell, H.: Active Sensing of CO_2 Emissions over Nights, Days, and Seasons (ASCENDS), American Geophysical Union, San Francisco, available at: http://adsabs.harvard.edu/abs/2007AGUFM.A11F..08D, 2007. 4537

Fisher, M. and Courtier, P.: Estimating the covariance matrices of analysis and forecast error in variational data assimilation, in: ECMWF Technical Memorandum 220, ECMWF, Reading, UK, 1995. 4550

ACPD
13, 4535–4600, 2013

Guerlet, S., Butz, A., Schepers, D., Basu, S., Hasekamp, O., Kuze, A., Yokota, T., Blavier, J.-F., Deutscher, N., Griffith, D., Hase, F., Kyrö, E., Morino, I., Sherlock, V., Sussman, R., Galli, A., and Aben, I.: Impact of aerosols and thin cirrus on retrieving and validating XCO_2 from GOSAT shortwave infrared measurements, J. Geophys. Res. Atmos., in review, 2013. 4539, 4543, 4556

Gurney, K. R.: Transcom 3 inversion intercomparison: model mean results for the estimation of seasonal carbon sources and sinks, Global Biogeochem. Cy., 18, doi:10.1029/2003GB002111, 2004. 4536, 4566, 4570

Gurney, K. R., Law, R. M., Denning, A. S., Rayner, P. J., Baker, D., Bousquet, P., Bruhwiler, L., Chen, Y.-H., Ciais, P., Fan, S., Fung, I. Y., Gloor, M., Heimann, M., Higuchi, K., John, J., Maki, T., Maksyutov, S., Masarie, K., Peylin, P., Prather, M., Pak, B. C., Randerson, J., Sarmiento, J., Taguchi, S., Takahashi, T., and Yuen, C.-W.: Towards robust regional estimates of CO_2 sources and sinks using atmospheric transport models, Nature, 415, 626–630, doi:10.1038/415626a, 2002. 4566, 4570

Gurney, K. R., Baker, D., Rayner, P., and Denning, S.: Interannual variations in continental-scale net carbon exchange and sensitivity to observing networks estimated from atmospheric CO_2 inversions for the period 1980 to 2005, Global Biogeochem. Cy., 22, GB3025, doi:10.1029/2007GB003082, 2008. 4536

Hamazaki, T., Kaneko, Y., and Kuze, A.: Carbon dioxide monitoring from the GOSAT satellite, in: Proceedings of the XXth ISPRS Conference, 2004. 4537

Houweling, S., Breon, F.-M., Aben, I., Rödenbeck, C., Gloor, M., Heimann, M., and Ciais, P.: Inverse modeling of CO_2 sources and sinks using satellite data: a synthetic inter-comparison of measurement techniques and their performance as a function of space and time, Atmos. Chem. Phys., 4, 523–538, doi:10.5194/acp-4-523-2004, 2004. 4537

Hungershoefer, K., Breon, F.-M., Peylin, P., Chevallier, F., Rayner, P., Klonecki, A., Houweling, S., and Marshall, J.: Evaluation of various observing systems for the global monitoring of CO_2 surface fluxes, Atmos. Chem. Phys., 10, 10503–10520, doi:10.5194/acp-10-10503-2010, 2010. 4537, 4539

Jacobson, A. R., Mikaloff Fletcher, S. E., Gruber, N., Sarmiento, J. L., and Gloor, M.: A joint atmosphere-ocean inversion for surface fluxes of carbon dioxide: 1. Methods and global-scale fluxes, Global Biogeochem. Cy., 21, GB1019, doi:10.1029/2005GB002556, 2007. 4546

ACPD
13, 4535–4600, 2013

Kaminski, T., Rayner, P. J., Heimann, M., and Enting, I. G.: On aggregation errors in atmospheric transport inversions, J. Geophys. Res., 106, 4703–4715, doi:10.1029/2000JD900581, 2001. 4543

Keppel-Aleks, G., Wennberg, P. O., Washenfelder, R. A., Wunch, D., Schneider, T., Toon, G. C., Andres, R. J., Blavier, J.-F., Connor, B., Davis, K. J., Desai, A. R., Messerschmidt, J., Notholt, J., Roehl, C. M., Sherlock, V., Stephens, B. B., Vay, S. A., and Wofsy, S. C.: The imprint of surface fluxes and transport on variations in total column carbon dioxide, Biogeosciences, 9, 875–891, doi:10.5194/bg-9-875-2012, 2012. 4539

Kettle, H. and Merchant, C. J.: Systematic errors in global air-sea CO_2 flux caused by temporal averaging of sea-level pressure, Atmos. Chem. Phys., 5, 1459–1466, doi:10.5194/acp-5-1459-2005, 2005. 4546

Krol, M., Houweling, S., Bregman, B., van den Broek, M., Segers, A., van Velthoven, P., Peters, W., Dentener, F., and Bergamaschi, P.: The two-way nested global chemistry-transport zoom model TM5: algorithm and applications, Atmos. Chem. Phys., 5, 417–432, doi:10.5194/acp-5-417-2005, 2005. 4547

Kulawik, S. S., Jones, D. B. A., Nassar, R., Irion, F. W., Worden, J. R., Bowman, K. W., Machida, T., Matsueda, H., Sawa, Y., Biraud, S. C., Fischer, M. L., and Jacobson, A. R.: Characterization of Tropospheric Emission Spectrometer (TES) CO_2 for carbon cycle science, Atmos. Chem. Phys., 10, 5601–5623, doi:10.5194/acp-10-5601-2010, 2010. 4537

Kuze, A., Suto, H., Nakajima, M., and Hamazaki, T.: Thermal and near infrared sensor for carbon observation Fourier-transform spectrometer on the Greenhouse gases observing satellite for greenhouse gases monitoring, Appl. Optics, 48, 6716–6733, doi:10.1364/AO.48.006716, 2009. 4538

Lanczos, C.: An iteration method for the solution of the eigenvalue problem of linear differential and integral operators, J. Res. Nat. Bur. Stand., 45, 255–282 1950. 4550

Machida, T., Matsueda, H., Sawa, Y., Nakagawa, Y., Hirotani, K., Kondo, N., Goto, K., Nakazawa, T., Ishikawa, K., and Ogawa, T.: Worldwide measurements of atmospheric CO_2 and other trace gas species using commercial airlines, J. Atmos. Ocean. Tech., 25, 1744–1754, doi:10.1175/2008JTECHA1082.1, 2008. 4552

Maki, T., Ikegami, M., Fujita, T., Hirahara, T., Yamada, K., Mori, K., Takeuchi, A., Tsutsumi, Y., Suda, K., and Conway, T.: New technique to analyse global distributions of CO_2 concentrations and fluxes from non-processed observational data, Tellus B, 62, 797–809, doi:10.1111/j.1600-0889.2010.00488.x, 2011. 4536

ACPD
13, 4535–4600, 2013

Meirink, J. F., Bergamaschi, P., and Krol, M. C.: Four-dimensional variational data assimilation for inverse modelling of atmospheric methane emissions: method and comparison with synthesis inversion, Atmos. Chem. Phys., 8, 6341–6353, doi:10.5194/acp-8-6341-2008, 2008. 4544, 4550

Messerschmidt, J., Parazoo, N., Deutscher, N. M., Roehl, C., Warneke, T., Wennberg, P. O., and Wunch, D.: Evaluation of atmosphere-biosphere exchange estimations with TCCON measurements, Atmos. Chem. Phys. Discuss., 12, 12759–12800, doi:10.5194/acpd-12-12759-2012, 2012. 4567

Miller, C. E., Crisp, D., DeCola, P. L., Olsen, S. C., Randerson, J. T., Michalak, A. M., Alkhaled, A., Rayner, P., Jacob, D. J., Suntharalingam, P., Jones, D. B. A., Denning, A. S., Nicholls, M. E., Doney, S. C., Pawson, S., Boesch, H., Connor, B. J., Fung, I. Y., O'Brien, D., Salawitch, R. J., Sander, S. P., Sen, B., Tans, P., Toon, G. C., Wennberg, P. O., Wofsy, S. C., Yung, Y. L., and Law, R. M.: Precision requirements for space-based X_{CO_2} data, J. Geophys. Res., 112, D10314, doi:10.1029/2006JD007659, 2007. 4537

Mueller, K. L., Gourdji, S. M., and Michalak, A. M.: Global monthly averaged CO_2 fluxes recovered using a geostatistical inverse modeling approach: 1. Results using atmospheric measurements, J. Geophys. Res., 113, 1–15, doi:10.1029/2007JD009734, 2008. 4536

Myhre, G., Alterskjaer, K., and Lowe, D.: A fast method for updating global fossil fuel carbon dioxide emissions, Environ. Res. Lett., 4, 34012, doi:10.1088/1748-9326/4/3/034012, 2009. 4546

Nassar, R., Jones, D. B. A., Kulawik, S. S., Worden, J. R., Bowman, K. W., Andres, R. J., Suntharalingam, P., Chen, J. M., Brenninkmeijer, C. A. M., Schuck, T. J., Conway, T. J., and Worthy, D. E.: Inverse modeling of CO_2 sources and sinks using satellite observations of CO_2 from TES and surface flask measurements, Atmos. Chem. Phys., 11, 6029–6047, doi:10.5194/acp-11-6029-2011, 2011. 4538

Navon, I. and Legler, D. M.: Conjugate-gradient methods for large-scale minimization in meteorology, Mon. Weather Rev., 115, 1479–1502, 1987. 4550

Niwa, Y., Machida, T., Sawa, Y., Matsueda, H., Schuck, T. J., Brenninkmeijer, C. A. M., Imasu, R., and Satoh, M.: Imposing strong constraints on tropical terrestrial CO_2 fluxes using passenger aircraft based measurements, J. Geophys. Res., 117, D11303, doi:10.1029/2012JD017474, 2012. 4552

ACPD
13, 4535–4600, 2013

Olsen, S. C. and Randerson, J. T.: Differences between surface and column atmospheric CO_2 and implications for carbon cycle research, J. Geophys. Res., 109, D02301, doi:10.1029/2003JD003968, 2004. 4546

Oshchepkov, S., Bril, A., Yokota, T., Morino, I., Yoshida, Y., Matsunaga, T., Belikov, D., Wunch, D., Wennberg, P., Toon, G., O'Dell, C., Butz, A., Guerlet, S., Cogan, A., Boesch, H., Eguchi, N., Deutscher, N., Griffith, D., Macatangay, R., Notholt, J., Sussmann, R., Rettinger, M., Sherlock, V., Robinson, J., Kyrö, E., Heikkinen, P., Feist, D. G., Nagahama, T., Kadygrov, N., Maksyutov, S., Uchino, O., and Watanabe, H.: Effects of atmospheric light scattering on spectroscopic observations of greenhouse gases from space: validation of PPDF-based CO_2 retrievals from GOSAT, J. Geophys. Res., 117, D12305, doi:10.1029/2012JD017505, 2012. 4556

Park, B. C. and Prather, M. J.: CO_2 source inversions using satellite observations of the upper troposphere, Geophys. Res. Lett., 28, 4571–4574, doi:10.1029/2001GL013604, 2001. 4537

Patra, P. K., Law, R. M., Peters, W., Rödenbeck, C., Takigawa, M., Aulagnier, C., Baker, I., Bergmann, D. J., Bousquet, P., Brandt, J., Bruhwiler, L., Cameron-Smith, P. J., Christensen, J. H., Delage, F., Denning, A. S., Fan, S., Geels, C., Houweling, S., Imasu, R., Karstens, U., Kawa, S. R., Kleist, J., Krol, M. C., Lin, S.-J., Lokupitiya, R., Maki, T., Maksyutov, S., Niwa, Y., Onishi, R., Parazoo, N., Pieterse, G., Rivier, L., Satoh, M., Serrar, S., Taguchi, S., Vautard, R., Vermeulen, A. T., and Zhu, Z.: TransCom model simulations of hourly atmospheric CO_2: Analysis of synoptic-scale variations for the period 2002–2003, Global Biogeochem. Cy., 22, GB4013, doi:10.1029/2007GB003081, 2008. 4541

Peters, W., Jacobson, A. R., Sweeney, C., Andrews, A. E., Conway, T. J., Masarie, K., Miller, J. B., Bruhwiler, L. M. P., Pétron, G., Hirsch, A. I., Worthy, D. E. J., Werf, G. R. V. D., Randerson, J. T., Wennberg, P. O., Krol, M. C., and Tans, P. P.: An atmospheric perspective on North American carbon dioxide exchange: CarbonTracker, P. Natl. Acad. Sci. USA, 104, 18925–18930, 2007. 4536, 4541, 4545

Peters, W., Krol, M. C., van Der Werf, G. R., Houweling, S., Jones, C. D., Hughes, J., Schaefer, K., Masarie, K. A., Jacobson, A. R., Miller, J. B., Cho, C. H., Ramonet, M., Schmidt, M., Ciattaglia, L., Apadula, F., Heltai, D., Meinhardt, F., di Sarra, A. G., Piacentino, S., Sferlazzo, D., Aalto, T., Hatakka, J., Ström, J., Haszpra, L., Meijer, H. A. J., van Der Laan, S., Neubert, R. E. M., Jordan, A., Rodó, X., Morguí, J. A., Vermeulen, A. T., Popa, E., Rozanski, K., Zimnoch, M., Manning, A. C., Leuenberger, M., Uglietti, C., Dolman, A. J., Ciais, P., Heimann, M., and Tans, P. P.: Seven years of recent European net terrestrial carbon diox-

ACPD
13, 4535–4600, 2013

ide exchange constrained by atmospheric observations, Glob. Change Biol., 16, 1317–1337, doi:10.1111/j.1365-2486.2009.02078.x, 2010. 4541

Rayner, P. J. and O'Brien, D. M.: The utility of remotely sensed CO_2 concentration data in surface source inversions, Geophys. Res. Lett., 28, 175–178, doi:10.1029/2000GL011912, 2001. 4537

Reuter, M., Bovensmann, H., Buchwitz, M., Burrows, J. P., Connor, B. J., Deutscher, N. M., Griffith, D. W. T., Heymann, J., Keppel-Aleks, G., Messerschmidt, J., Notholt, J., Petri, C., Robinson, J., Schneising, O., Sherlock, V., Velazco, V., Warneke, T., Wennberg, P. O., and Wunch, D.: Retrieval of atmospheric CO_2 with enhanced accuracy and precision from SCIAMACHY: validation with FTS measurements and comparison with model results, J. Geophys. Res., 116, D04301, doi:10.1029/2010JD015047, 2011. 4537

Rödenbeck, C., Houweling, S., Gloor, M., and Heimann, M.: CO_2 flux history 1982–2001 inferred from atmospheric data using a global inversion of atmospheric transport, Atmos. Chem. Phys., 3, 1919–1964, doi:10.5194/acp-3-1919-2003, 2003. 4536

Sawa, Y., Machida, T., and Matsueda, H.: Aircraft observation of the seasonal variation in the transport of CO_2 in the upper atmosphere, J. Geophys. Res., 117, D05305, doi:10.1029/2011JD016933, 2012. 4552

Scholes, R. J., Monteiro, P. M. S., Sabine, C. L., and Canadell, J. G.: Systematic long-term observations of the global carbon cycle, Trends Ecol. Evol., 24, 427–430, doi:10.1016/j.tree.2009.03.006, 2009. 4537

Stephens, B. B., Gurney, K. R., Tans, P. P., Sweeney, C., Peters, W., Bruhwiler, L., Ciais, P., Ramonet, M., Bousquet, P., Nakazawa, T., Aoki, S., Machida, T., Inoue, G., Vinnichenko, N., Lloyd, J., Jordan, A., Heimann, M., Shibistova, O., Langenfelds, R. L., Steele, L. P., Francey, R. J., and Denning, A. S.: Weak northern and strong tropical land carbon uptake from vertical profiles of atmospheric CO_2, Science, 316, 1732–1735, doi:10.1126/science.1137004, 2007. 4566, 4567, 4570

Tans, P. P., Fung, I. Y., and Takahashi, T.: Observational Contrains on the Global Atmospheric CO_2 Budget, Science, 247, 1431–1438, doi:10.1126/science.247.4949.1431, 1990. 4536, 4566, 4567, 4570

Tarantola, A.: Inverse Problem Theory, SIAM, Philadelphia, 2005. 4550

Thoning, K. W., Tans, P. P., and Komhyr, W. D.: Atmospheric carbon dioxide at mauna loa observatory, 2. Analysis of the NOAA GMCC data, 1974–1985, J. Geophys. Res., 94, 8549–8565, doi:10.1029/JD094iD06p08549, 1989. 4565

ACPD
13, 4535–4600, 2013

van der Werf, G. R., Randerson, J. T., Giglio, L., Collatz, G. J., Mu, M., Kasibhatla, P. S., Morton, D. C., DeFries, R. S., Jin, Y., and van Leeuwen, T. T.: Global fire emissions and the contribution of deforestation, savanna, forest, agricultural, and peat fires (1997–2009), Atmos. Chem. Phys., 10, 11707–11735, doi:10.5194/acp-10-11707-2010, 2010. 4546

Wang, H., Jacob, D. J., Kopacz, M., Jones, D. B. A., Suntharalingam, P., Fisher, J. A., Nassar, R., Pawson, S., and Nielsen, J. E.: Error correlation between CO_2 and CO as constraint for CO_2 flux inversions using satellite data, Atmos. Chem. Phys., 9, 7313–7323, doi:10.5194/acp-9-7313-2009, 2009. 4554

Wunch, D., Toon, G. C., Wennberg, P. O., Wofsy, S. C., Stephens, B. B., Fischer, M. L., Uchino, O., Abshire, J. B., Bernath, P., Biraud, S. C., Blavier, J.-F. L., Boone, C., Bowman, K. P., Browell, E. V., Campos, T., Connor, B. J., Daube, B. C., Deutscher, N. M., Diao, M., Elkins, J. W., Gerbig, C., Gottlieb, E., Griffith, D. W. T., Hurst, D. F., Jiménez, R., Keppel-Aleks, G., Kort, E. A., Macatangay, R., Machida, T., Matsueda, H., Moore, F., Morino, I., Park, S., Robinson, J., Roehl, C. M., Sawa, Y., Sherlock, V., Sweeney, C., Tanaka, T., and Zondlo, M. A.: Calibration of the Total Carbon Column Observing Network using aircraft profile data, Atmos. Meas. Tech., 3, 1351–1362, doi:10.5194/amt-3-1351-2010, 2010. 4553

Wunch, D., Toon, G., Blavier, J.-F., Washenfelder, R., Notholt, J., Connor, B., Griffith, D., Sherlock, V., and Wennberg, P.: The total carbon column observing network (TCCON), Philos. T. Roy. Soc. A, 369, 2087–2112, doi:10.1098/rsta.2010.0240, 2011. 4539, 4553

Yang, Z., Washenfelder, R. A., Keppel-Aleks, G., Krakauer, N. Y., Randerson, J. T., Tans, P. P., Sweeney, C., and Wennberg, P. O.: New constraints on Northern Hemisphere growing season net flux, Geophys. Res. Lett., 34, 1–6, doi:10.1029/2007GL029742, 2007. 4539, 4554, 4567

ACPD
13, 4535–4600, 2013

Table 1. Covariance parameters in Eq. (4) for different categories.

Category	L (km)	T (months)	ξ
Biosphere flux	500	3	0.84
Oceanic flux	3000	6	0.60

ACPD
13, 4535–4600, 2013

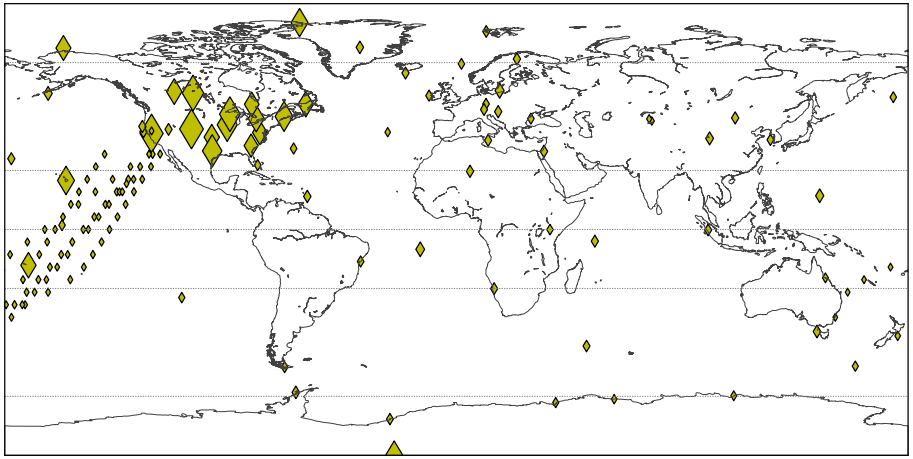

Fig. 1. Locations of the point samples assimilated in our inversions. The marker size represents the amount of observational data from each location assimilated in our inversions. For example, although there is a high density of location markers over the tropical Pacific, there are very few data points from each of those locations, since the data there come from one-time cruises.

ACPD
13, 4535–4600, 2013

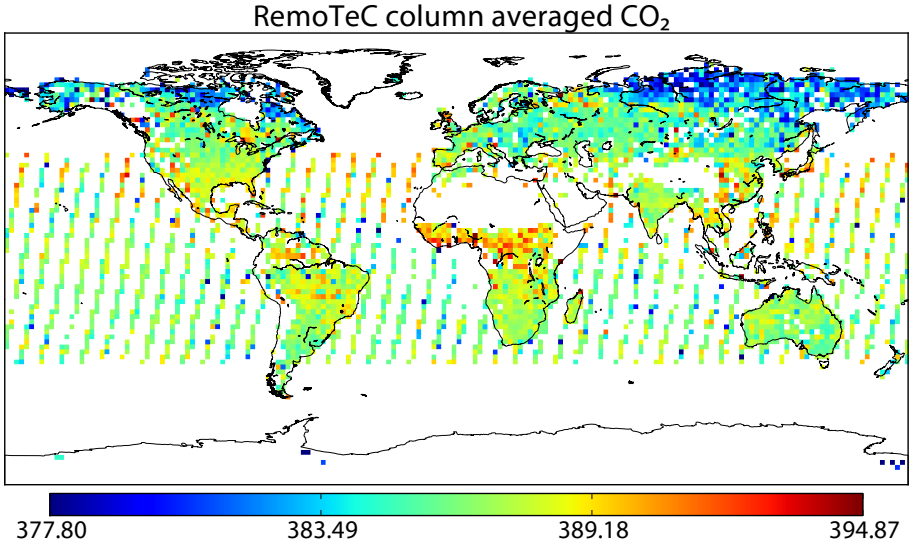

Fig. 2. GOSAT X_{CO_2} between 1 June 2009 and 1 January 2011, shown here averaged over a $2^\circ \times 2^\circ$ grid. The averaging is only for visual clarity; the data assimilation considered each observation individually. The color of a grid box represents the average X_{CO_2} within that grid box, in mole fraction of dry air expressed as parts per million.

ACPD
13, 4535–4600, 2013

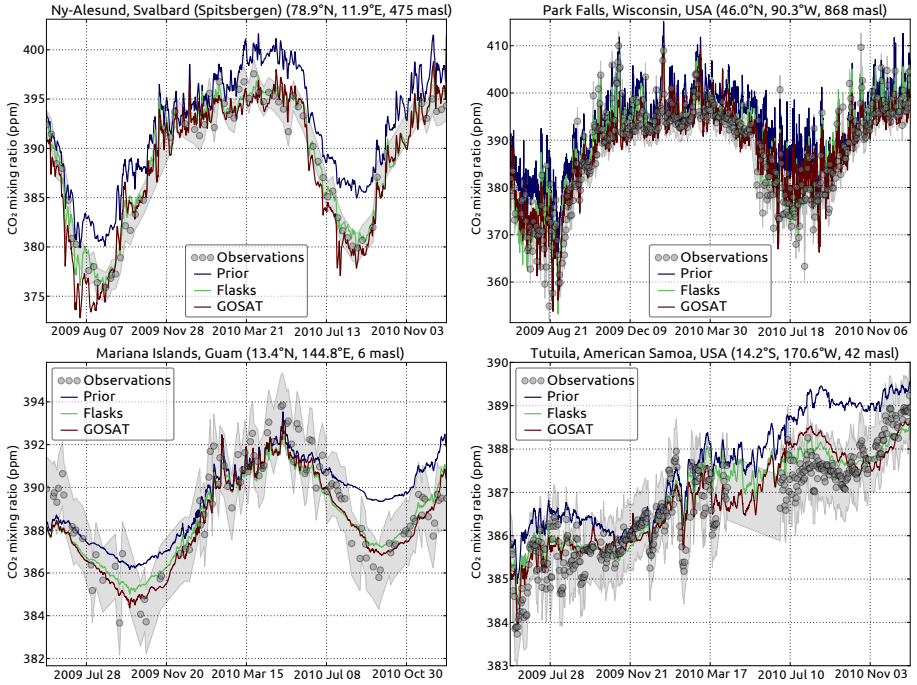

Fig. 3. Model estimated CO_2 time series at four surface stations in the tropics and northern extra-tropics, compared to CO_2 measurements taken at those stations. The "GOSAT" line is from an inversion using only GOSAT X_{CO_2}, whereas the "Flasks" line is from an inversion using only surface samples.

ACPD
13, 4535–4600, 2013

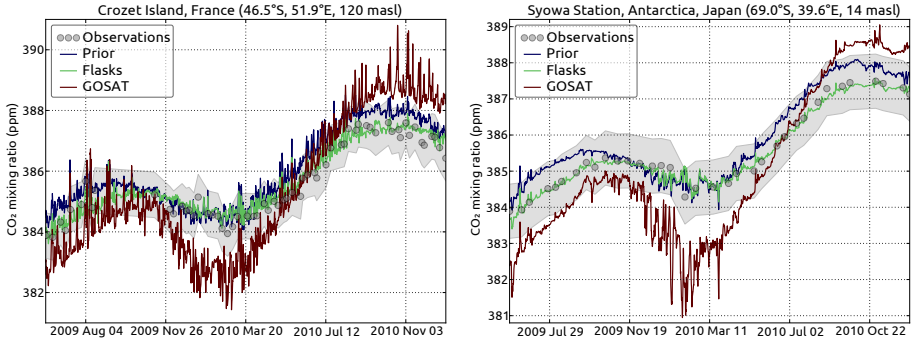

Fig. 4. Model estimated CO_2 time series at two surface stations in the southern extra-tropics, compared to CO_2 measurements taken at those stations. The "GOSAT" line is from an inversion using only GOSAT X_{CO_2}, whereas the "Flasks" line is from an inversion using only surface samples.

ACPD
13, 4535–4600, 2013

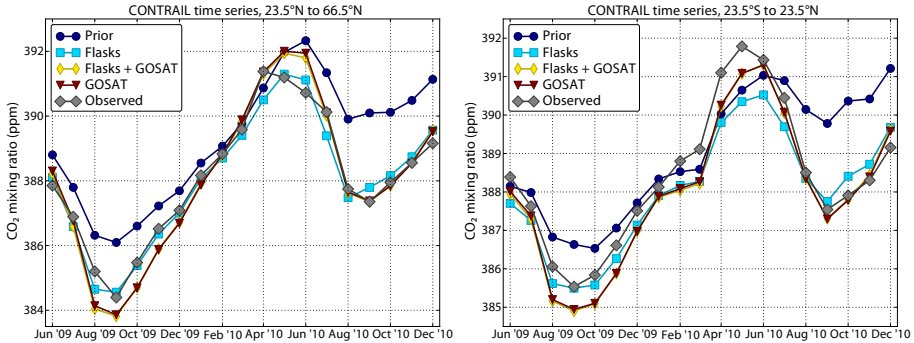

Fig. 5. Monthly averaged CONTRAIL data between (left) 23.5° N and 66.5° N and (right) 23.5° S and 23.5° N, along with posterior CO_2 fields sampled at CONTRAIL sample points.

ACPD
13, 4535–4600, 2013

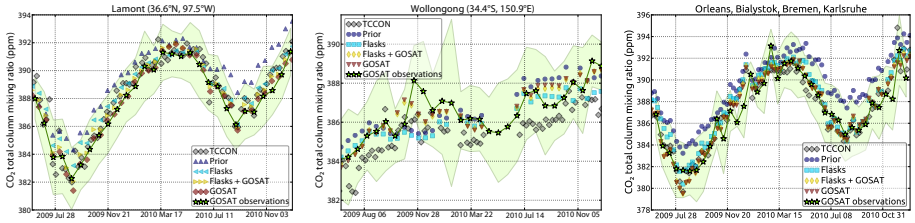

Fig. 6. 7-day averaged TCCON data at Lamont (left) and Wollongong (center), along with posterior CO_2 fields co-sampled and convolved with the respective averaging kernels. For each TCCON station, coincident GOSAT data have been averaged over 15 days – due to higher scatter – and plotted over. The shaded area is the standard deviation of all the coincident data for a month, i.e. it is the "error bar" region of the stars. Over Europe (right), due to gaps in TCCON data over individual stations, data from four stations have been combined, along with their corresponding coincident GOSAT data and posterior co-sampled X_{CO_2}.

ACPD
13, 4535–4600, 2013

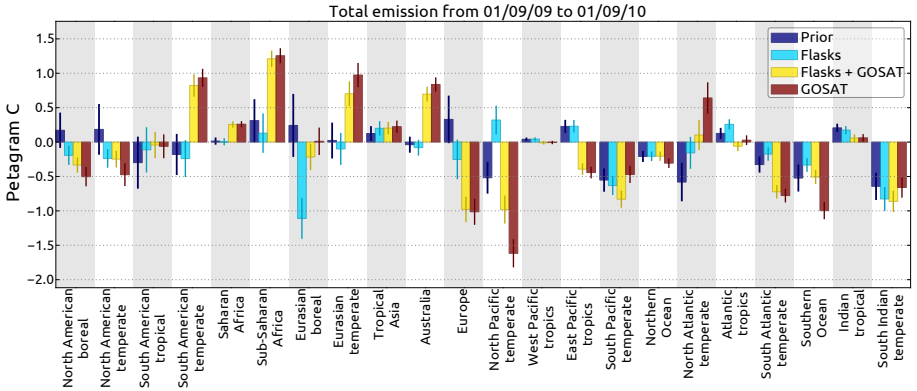

Fig. 7. Aggregated emission between 1 September 2009 and 1 September 2010 from the 22 TRANSCOM regions. The emission figures do not include fossil fuel emission. Error bars denote 1σ errors.

ACPD
13, 4535–4600, 2013

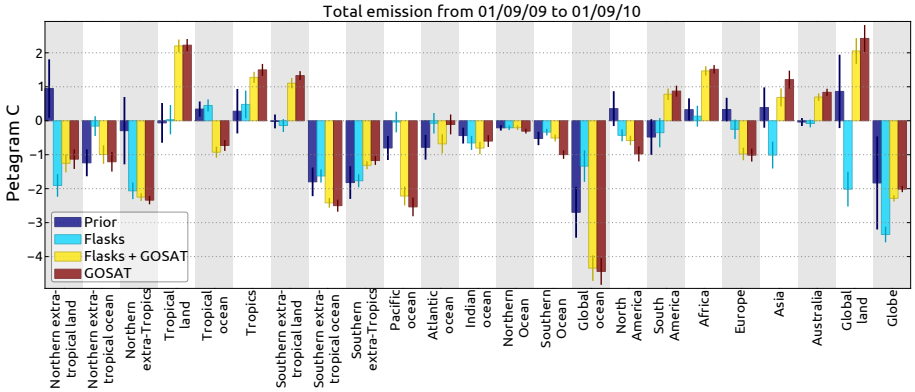

Fig. 8. Aggregated emission between 1 September 2009 and 1 September 2010, partitioned over larger regions such as different continents and latitude bands. The emission figures do not include fossil fuel emission. Error bars denote 1σ errors.

ACPD
13, 4535–4600, 2013

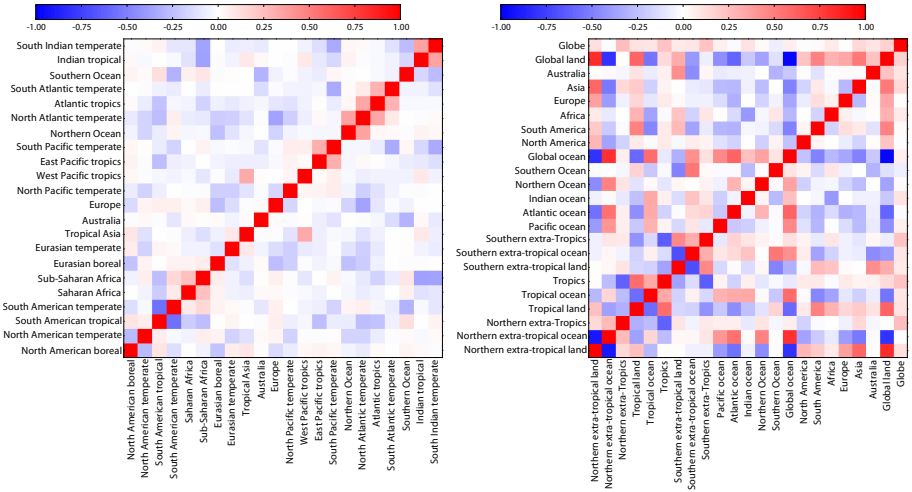

Fig. 9. The posterior correlation matrix between optimized emissions shown in Figs. 7 and 8. On the left are the 22 TRANSCOM regions, and on the right are larger regions comprised of several TRANSCOM regions. These matrices correspond to the inversion assimilating both GOSAT and surface layer CO_2 data.

ACPD
13, 4535–4600, 2013

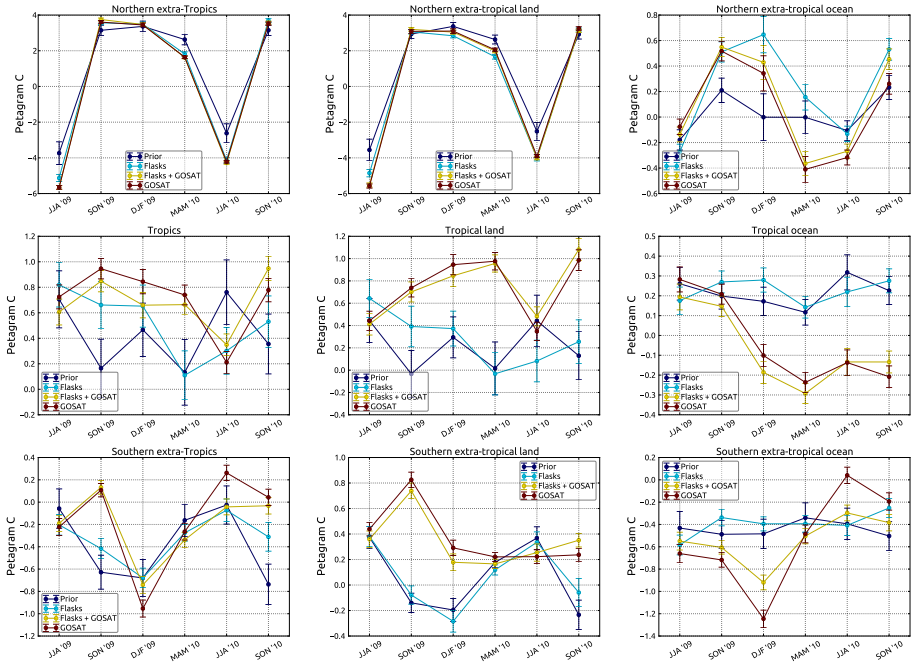

Fig. 10. Seasonal time series of the surface flux from the northern extra-tropics (top row), the tropics (middle row), and the southern extra-tropics (bottom row). The left column shows the total flux, the central column shows the terrestrial biosphere component, and the right column the oceanic contribution. In the northern extra-tropics, since the seasonal cycle imposed by the terrestrial biosphere is much larger than that imposed by the ocean, almost all of the Northern extra-tropical seasonal signal comes from the land. In the tropics and southern extra-tropics, the magnitude of the seasonal variation of the oceanic source/sink is comparable to that of the land source/sink, although the phasing is different.

ACPD
13, 4535–4600, 2013

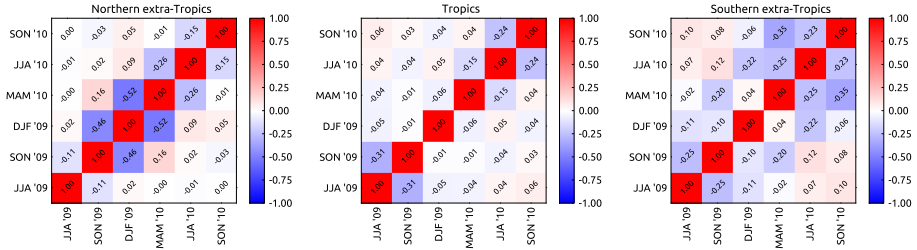

Fig. 11. The posterior temporal correlation between the flux adjustments made in different seasons for the three latitudinal bands represented in Fig. 10. The numbers in the cells are the posterior correlation coefficients.

ACPD
13, 4535–4600, 2013

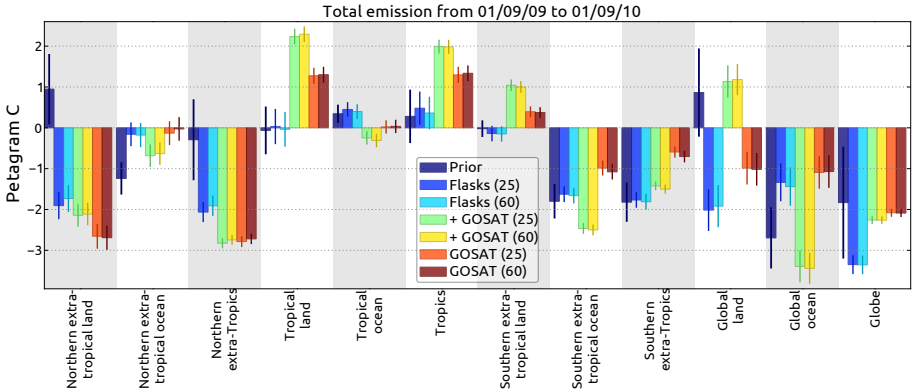

Fig. 12. Aggregated fluxes over different regions between 1 September 2009 and 1 September 2010, similar to Fig. 8. Each data source (surface data, GOSAT data) has been assimilated by running the TM5 transport model at two different vertical resolutions, 25 and 60 layers, which are indicated in the legend in parentheses.

ACPD
13, 4535–4600, 2013

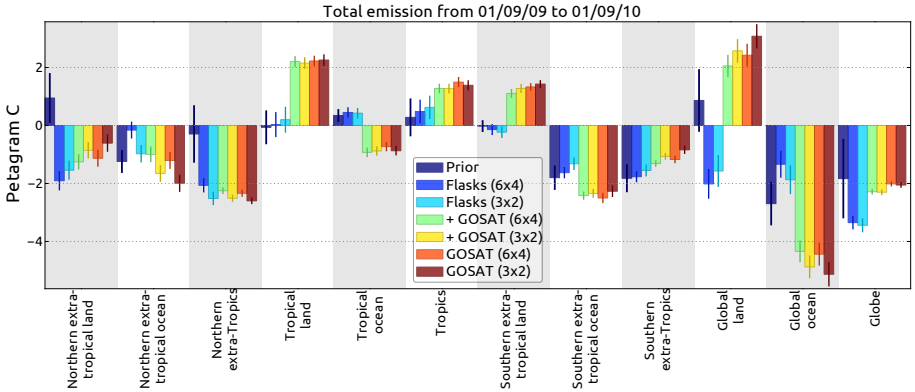

Fig. 13. Aggregated fluxes over different regions between 1 September 2009 and 1 September 2010, similar to Fig. 12. Each data source (surface data, GOSAT data) has been assimilated by running the TM5 transport model at two different horizontal resolutions, $3^\circ \times 2^\circ$ and $6^\circ \times 4^\circ$, which are indicated in the legend in parentheses.

ACPD
13, 4535–4600, 2013

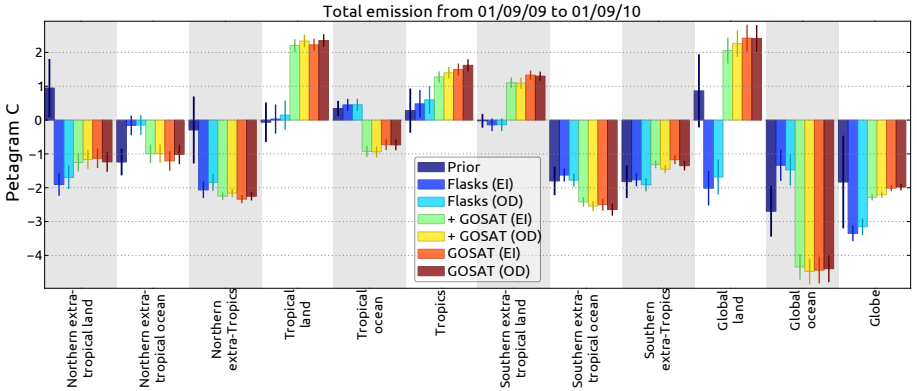

Fig. 14. Aggregated fluxes over different regions between 1 September 2009 and 1 September 2010, similar to Fig. 12. Each data source (surface data, GOSAT data) has been assimilated by running the TM5 transport model with two different assimilated meteorological data sets, ECMWF Era Interim ("EI" in the legend) and ECMWF operational forecasts ("OD" in the legend).

ACPD
13, 4535–4600, 2013

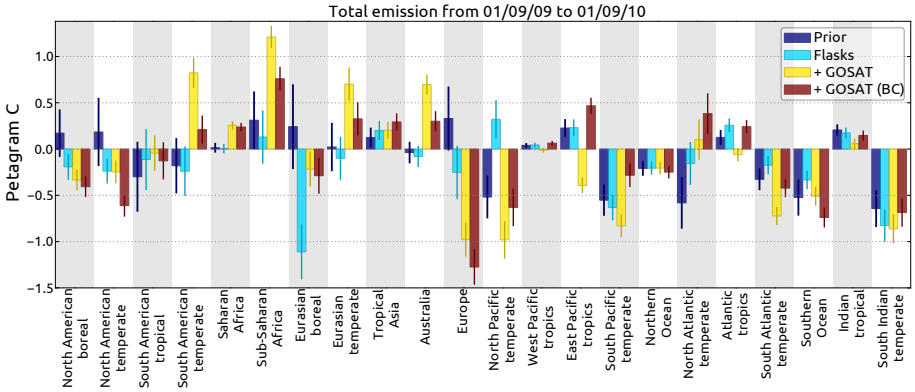

Fig. 15. The optimized flux over the 22 TRANSCOM regions from a joint inversion optimizing bias parameters defined in Eq. (7) (denoted "+ GOSAT (BC)"), compared to the joint inversion shown in Fig. 7 (denoted "+ GOSAT").

ACPD
13, 4535–4600, 2013

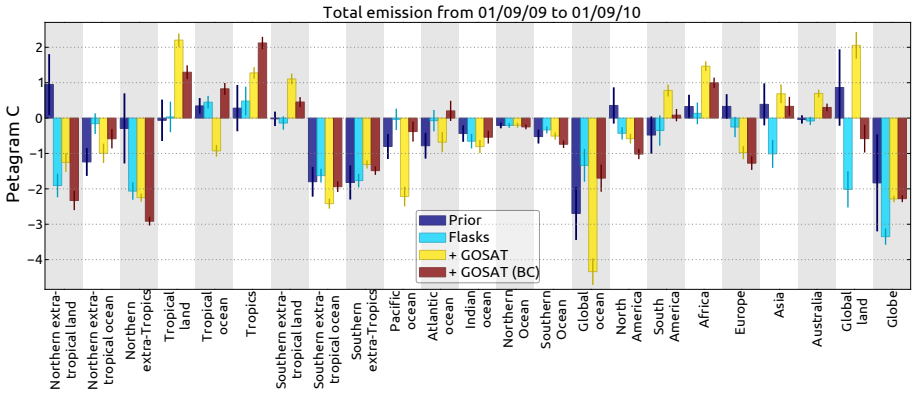

Fig. 16. The optimized flux over some large regions from a joint inversion optimizing bias parameters defined in Eq. (7) (denoted "+ GOSAT (BC)"), compared to the joint inversion shown in Fig. 8 (denoted "+ GOSAT").

ACPD
13, 4535–4600, 2013

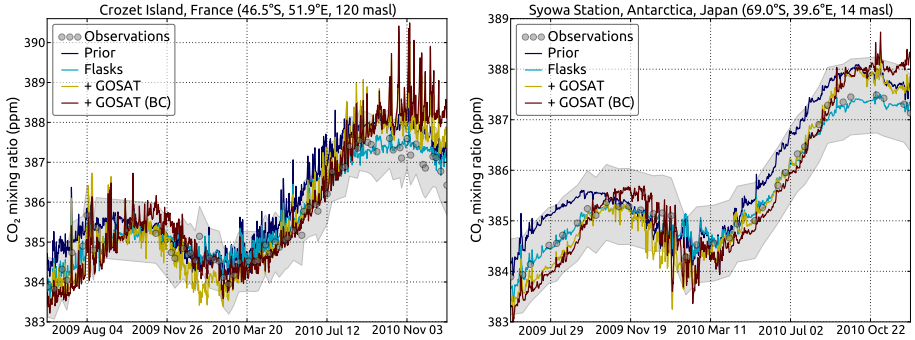

Fig. 17. The prior and posterior CO_2 time series at the same two southern extra-tropical stations as shown in Fig. 4. The inversion labeled "+ GOSAT (BC)" is a joint inversion in which a land-ocean bias in GOSAT X_{CO_2} data has been optimized for, whereas the inversion labeled "+ GOSAT" is a joint inversion without any bias correction. The optimized CO_2 time series at the surface in the SH extra-tropics from "+ GOSAT (BC)" has a lower seasonal cycle amplitude compared to "+ GOSAT".

ACPD
13, 4535–4600, 2013

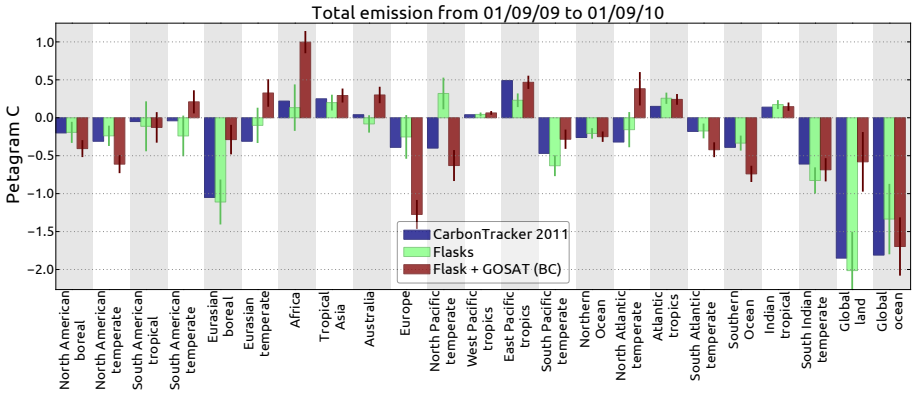

Fig. 18. Comparison of our optimized fluxes with those from CarbonTracker 2011 over the TRANSCOM regions and the global land and ocean. All fluxes are without fossil fuel emissions. Since TRANSCOM regions include Northern and Southern Africa, whereas we aggregate over Saharan and sub-Saharan Africa (Fig. 7) in this figure we have presented the flux total over Africa.

ACPD
13, 4535–4600, 2013

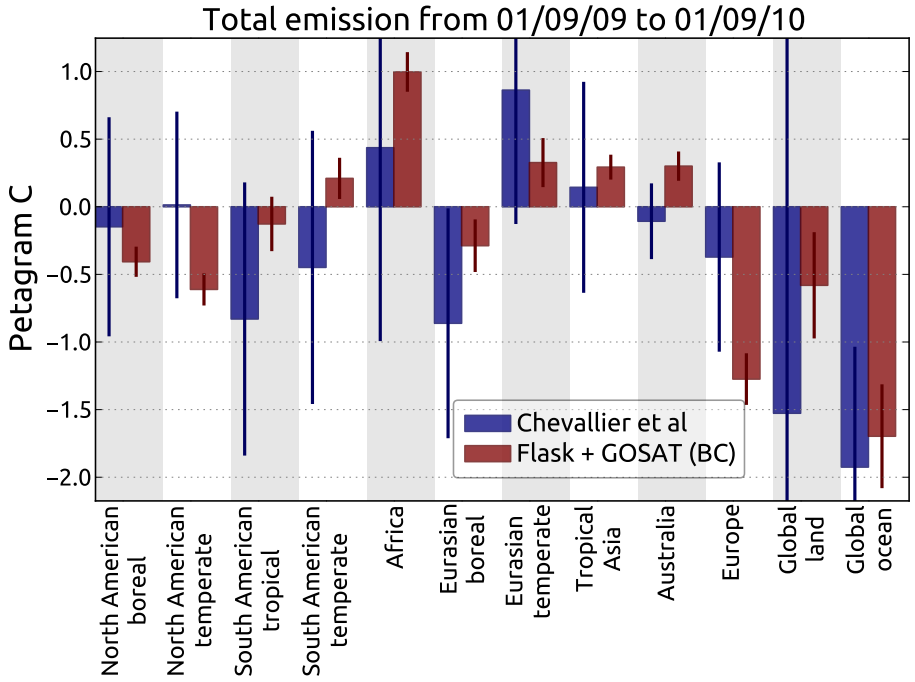

Fig. 19. Comparison of our optimized fluxes over aggregated land areas with those obtained by Chevallier et al. (2011) after assimilating TCCON X_{CO_2}. Both sets of fluxes are without fossil fuel emissions.

ACPD
13, 4535–4600, 2013